FoxG1 antagonizes neocortical stem cell progression to astrogenesis

Title

Foxg1 antagonizes neocortical stem cell progression to astrogenesis

Authors

Carmen Falcone [1,2], Manuela Santo [1], Gabriele Liuzzi [1], Noemi Cannizzaro [1], Clara Grudina [1,,3], Erica Valencic [4], Luca Peruzzotti-Jametti [5], Stefano Pluchino [5], Antonello Mallamaci [1,*]

Affiliations

[1] Laboratory of Cerebral Cortex Development, Neuroscience Area, SISSA, Trieste, Italy

[2] *present address:* Institute for Pediatric Regenerative Medicine and Shriners Hospitals for Children Northern California, UC Davis, Sacramento, CA, USA

[3] *present address:* Istitut Pasteur, Paris, France

[4] Department of Diagnostics, Institute for Maternal and Child Health, IRCCS Burlo Garofolo, Trieste, Italy

[5] Department of Clinical Neurosciences - Division of Stem Cell Neurobiology, Wellcome Trust-Medical Research Council Stem Cell Institute and NIHR Biomedical Research Centre, University of Cambridge, UK

[*] corresponding author [address: via Bonomea 265 - 34136 Trieste - Italy; phone: +39 040 3787 717; e-mail: amallama@sissa.it]

Running title

Foxg1 antagonizes neocortical astrogenesis

ABSTRACT

Neocortical astrogenesis follows neuronogenesis and precedes oligogenesis. Among key factors dictating its temporal articulation, there are progression rates of pallial stem cells (SCs) towards astroglial lineages as well as activation rates of astrocyte differentiation programs in response to extrinsic gliogenic cues. In this study, we showed that high Foxg1 SC expression antagonizes astrocyte generation, while stimulating SC self-renewal and committing SCs to neuronogenesis. We found that mechanisms underlying this activity are mainly cell autonomous and highly pleiotropic. They include a concerted downregulation of four key effectors channelling neural SCs to astroglial fates, as well as defective activation of core molecular machineries implementing astroglial differentiation programs. Next, we found that SC Foxg1 levels specifically decline during the neuronogenic-to-gliogenic transition, pointing to a pivotal Foxg1 role in temporal modulation of astrogenesis. Finally, we showed that Foxg1 inhibits astrogenesis from human neocortical precursors, suggesting that this is an evolutionarily ancient trait.

KEYWORDS

Foxg1, astrogenesis, NSC, commitment, differentiation

Neocortical astrocytes are generated according to a peculiar, spatio-temporal and clonal pattern. They originate from neural precursors located in neopallial periventricular layers (Gorski et al. 2002; Tsai et al. 2012), largely via committed progenitors. Still intermitotic, these progenitors migrate towards more marginal layers, where they locally proliferate and give rise to mature differentiated progenies (Ge et al. 2012; Magavi et al. 2012) Astrogenesis initiates at low levels at mid-neuronogenic stages and peaks up after neuronogenesis completion (Okano and Temple 2009). Clonal trees originating from isolated, early pallial stem cells reveal the early occurrence of neuronal progenitors and later appearance of glia- and astroglia-committed precursors (Qian et al. 2000). All these precursors are detectable *in vivo* along a largely consistent temporal progression (Costa et al. 2009).

Among processes dictating the ultimate neocortical astroglial output there is the transition from early neural stem cells (NSCs) to astrocyte-committed progenitors, namely a key developmental step requiring an accurate molecular control. This control is exerted by a large set of genes, most of which have been implicated in a dense and intricate functional network (Mallamaci 2013; Kanski et al. 2014; Sloan and Barres 2014; Takouda et al. 2017). A small group of transcription factors, including CouptfI/II, Zbtb20, Sox9 and Nfia, promote the astrogenesis onset, partly by changing the epigenetic state of astroglial genes (Naka et al. 2008; Namihira et al. 2009; Kang et al. 2012; Nagao et al. 2016). Once chromatin of genes active in astroglia gets permissive, then its transcription rate results from the interaction among dedicated signalling pathways, impinging on astroglial promoters. Some of them inhibit astroglial gene transcription (e.g. Nrg1/ErbB4^{ICD}-NCoR (Hermanson et al. 2002; Sardi et al. 2006; Schlessinger and Lemmon 2006; Miller and Gauthier 2007)), some others promote it (e.g. IL6/Jak2/Stat1,3 (Derouet et al. 2004; Barnabé-Heider et al. 2005; He et al. 2005), Bmp/Smad1,5,8 (Nakashima 1999; Sun et al. 2001), Dll1/Notch1^{ICD} (Ge et al. 2002; Kamakura et al. 2004).

We previously found that pallial NSC-restricted overexpression of *Foxg1*, an ancient transcription factor controlling telencephalic specification (Hanashima et al. 2007), subpallial/pallial fate (Manuel et al. 2010; Mariani et al. 2015; Patriarchi et al. 2016), hippocampal programs (Muzio and Mallamaci 2005)and neuronogenesis progression (Chiola et al. in press; Miyoshi and Fishell 2012; Toma et al. 2014), leads to a substantial decrease of astrocyte generation (Brancaccio et al. 2010). However, we demonstrated the occurrence of this phenomenon only in a murine, heterochronic *in vitro* system, we did not address its physiological relevance and, last, we did not focus on molecular mechanisms underlying it (Brancaccio et al. 2010).

In this study we showed that *Foxg1* overexpression within neocortical stem cells commits these cells to neuronogenesis rather than astrogenesis, *in vivo* as well as *in vitro*, both in mouse and human. Interestingly, we found that *Foxg1* inhibition of astrogenesis stems from variegated mechanisms. These include a direct trans-repression of genes biasing neural stem cells to astroglial fates, as well as an articulated impact on key pathways

which modulate astroglial gene transcription, resulting into a robust dampening of it. Finally, we provided evidence that Foxg1 levels decline, while neocortical NSCs move from neuronogenesis to gliogenesis.

These findings point to an evolutionarily conserved, pivotal role of *Foxg1* in fine temporal regulation of astrogenesis. They also suggest that neurological symptoms observed in syndromes with altered *Foxg1* allele dosage (Guerrini and Parrini 2012) might be partially caused by an unbalanced astrocyte generation.

MATERIALS AND METHODS

Animal Handling and Embryo Dissection

Animal handling and subsequent procedures were in accordance with European and Italian laws [European Parliament and Council Directive of September 22, 2010 (2010/63/EU); Italian Government Decree of March 04, 2014, n° 26]. Experimental protocols were approved by SISSA OpBA (Institutional SISSA Committee for Animal Care) and authorized by the Italian Ministery of Health (Auth. N° 1231/2015-PR of Nov 25, 2015).

Wild type (strain CD1, purchased from Envigo, Italy) and *Foxg1*$^{+/-}$ strain (Hébert and McConnell 2000) were maintained at the SISSA animal facility. Embryos were staged by timed breeding and vaginal plug inspection. Pregnant females were sacrificed by cervical dislocation. Embryonic cortices were dissected out in cold 1X-phosphate buffered saline (PBS), under sterile conditions.

Derivation of human neocortical precursor line

NPCs were derived from the cerebral cortex of a single 10.2 post conception week (PCW) human foetus, collected from routine termination of pregnancies under full ethical approval in line with Department of Health guidelines (LREC 96/085;96/085 - In vitro study of post-mortem human foetal neural tissue, blood and haematopoietic organs, approved by Cambridge Central Ethics Committee). Cells were grown and expanded in a chemically defined, serum-free medium in the presence of Fibroblast Growth Factor 2 (Fgf2) and Epidermal Growth Factor (Egf) (10 and 20 ng/ml, respectively) and routinely assessed for multipotency, as described (Pluchino et al. 2009).

Derivation of human neocortical precursor line, Lentiviral Vectors Packaging and Titration, Engineering cells for *in vivo* transplantation, *In vivo* neural precursor cell transplantation, Histology brain sample preparation, Cortical cultures, for differentiation assays, and mRNA profiling, Immunofluorescence analysis, Analytical cytofluorimetry: cell preparation and analysis, Preparative cytofluorimetry: cell preparation and sorting, RNA profiling: qRT-PCR, ChIP-qPCR.

They were performed according to standard protocols. Temporal articulation of protocols and molecular tools for their implementation are illustrated in dedicated figure panels (see Fig. 1-6 and S8). Full protocol details, including lists of lentiviruses, PCR oligo sequences and antibodies employed, are provided in Supplementary Materials

RESULTS

Foxg1 overexpression in murine neocortical neural stem cells antagonizes astrogenesis.

Previous investigations in our lab gave evidence for a reduction of the astroglial output following *Foxg1* overexpression in NSCs (Brancaccio et al. 2010). However, this phenomenon was only documented *in vitro*, as well as in a temporal frame *delayed* as compared to the standard astrogliogenic schedule (Okano and Temple 2009) Based on these findings, we hypothesized that *Foxg1* might also control the *physiological*, timed progression of neocortical neural stem cells towards glial fates. To test this hypothesis, we decided to assess if *Foxg1* overexpression impacts the *in vivo* astroglial output of genetically manipulated NSCs transplanted into *wild type* recipient brains, according to a developmentally plausible schedule. For this purpose, we engineered dissociated E12.5 cortico-cerebral precursors for conditional, TetON-driven *Foxg1* overexpression, under the control of a *Nestin* gene-derivative promoter (pNes) selectively firing in NSCs (Brancaccio et al. 2010). We acutely activated the transgene via doxycyclin administration and we maintained cells in a pro-proliferative medium for seven days. Then, we transplanted cells into the parietal cortico-cerebral parenchyma of P0 isochronic mouse pups. Specifically, we injected a 1:1 mix of cells, made alternatively gain-of-function (GOF) for *Foxg1* or a control, and labelled with EGFP and mCherry, respectively. Four days later, we sacrificed the pups and scored their brains for the astroglial outputs of the two different, transplanted precursor types (**Fig. 1 A,D).** For this purpose, we took advantage of S100β, a Ca^{2+}-binding protein shared by ependyma and glial lineages, mainly expressed by astroglial cells of perinatal neocortical tissue (Deloulme et al. 2004; Raponi et al. 2007; Falcone et al. 2015). We found that, compared to controls, $S100\beta^{+}$ derivatives of *Foxg1*-GOF cells were reduced by 19.25±6.94% ($p<9.60x10^{-6}$, n=8,8*, paired t-test*) (**Fig. 1E**, right, and **S1B**). As *Foxg1* also promotes NSCs self-renewal (Brancaccio et al., 2010), we reasoned that this might lead us to underestimate the actual impact of *Foxg1* overexpression on the NSC astrogenic bias. Therefore, to compensate for such an effect, first, we evaluated the frequency of $Nestin^{+}$ NSCs within sister cell preparations, engineered like the transplanted ones (but not labelled by EGFP or mCherry) and kept in pro-proliferative medium for 7 days (**Fig. 1 A,D**). Then, we normalized the *in vivo* astroglial output of transplanted cells against such frequency. We found that *Foxg1* overexpression induced a 2.5-folds increase of $Nestin^{+}$ cells (+149.76±6.34%, $p<4.55x10^{-7}$*,* n=3,3) (**Fig. 1E**, left, and **S1A**), meaning that the average, *NSCs-normalized* $S100\beta^{+}$ astrocytic output was decreased by as much as 67.67%.

To corroborate these results, we performed a specular loss-of-function assay, employing neural precursors alternatively engineered by an α*Foxg1-shRNA*-expressing-LV or a control (**Fig. 1B,D**). Here we expected an enlargement of the astroglial output. Consequently, to increase the sensitivity of the assay, we interrogated E12.5 precursor derivatives kept *in vitro* for only 4 days being therefore further from the astrogenic peak. Specifically, we co-transplanted these cells as 1:1 mixes into heterochronic P0 pups and-we assessed their final glial output at P4. The S100β$^+$ cells frequency did not change upon *Foxg1* manipulation (*n*=4,4) (**Fig. 1F,** right, and **S1D**). However, on the day of transplantation, the frequency of Nestin$^+$ cells was decreased by 32.14±3.26% ($p<1.12x10^{-3}$, *n*=3,3) in α*Foxg1-shRNA* samples compared to controls (**Fig. 1F,** left, and **S1C**). This means that αFoxg1-shRNA manipulation upregulated the average, *NSC-normalized* astrogenic output by 39.75%.

To further validate these results, we repeated our gain-of-function assay restricting the manipulation of *Foxg1* NSC levels to the *in vivo* environment. To this aim, we kept dissociated E11.5 cortico-cerebral precursors, made acutely *Foxg1*-GOF under pNes/TetON control, for three days in a doxy-free pro-proliferative medium. Then, we transplanted a 1:1 mix of these cells (EGFP-labelled) and their controls (mCherry-labelled) into the lateral ventricle of E14.5 isochronic mouse embryos. Last, we activated *Foxg1* and control transgenes via oral doxycyclin administration to pregnant females. We allowed the embryos to be born, we sacrificed the pups at P4, and we evaluated the astroglial outputs of the two different, transplanted precursor types **(Fig. 1C,D).** Similarly to the first *Foxg1*-GOF assay, we found that S100β$^+$ derivatives of *Foxg1*-GOF precursors were robustly reduced compared to controls (-24.08±11.03%, $p< 0.01$, *n*=4,4*, paired t-test*) (**Fig. 1G** and **S1E**), so definitively pointing to a genuine *Foxg1* anti-astrogenic activity.

To model molecular mechanisms underlying this activity, we considered to investigate them in dissociated neural cultures. To confirm the feasibility of this approach, we first verified if the outcome of *Foxg1* manipulation could be fully replicated in these cultures, within a biologically acceptable temporal framework. For this purpose, we engineered dissociated E12.5 cortico-cerebral precursors for conditional *Foxg1* overexpression as described above for transplantation assays, we maintained these cells in a pro-proliferative medium for seven days, and we allowed them to differentiate on poly-L-lysin-coated coverslips for four additional days. We kept the *Foxg1* transgene on during the entire procedure. Following *Foxg1* overactivation, we found a pronounced loss of S100β$^+$ astrocytes (-63.89±9.14%, $p<0.003$, *n*=4,4) as well as a consistent reduction of Gfap$^+$ cells (-37.32±20.10%, $p<0.002$, *n*=3,3) **(Fig. 1H,I** and **S1G,H)** [Gfap is an intermediate filament protein, mainly confined to astrocytes of rodent neocortex (Malatesta et al. 2008)]. Remarkably, this anti-differentiative effect was specific to the astroglial lineage, as, within the same cultures, the frequency of Tubβ3$^+$ neurons was almost doubled (+90.45±4.53%, $p<0.03$, *n*=3,3) **(Fig. 1H,I** and **S1I)**. In a second test, astroglial cultures were conversely prepared from *Foxg1*$^{+/-}$ (Hébert and McConnell 2000) mice-derived cortico-cerebral precursors. In this case, no S100β$^+$ output change was detected compared to *wild type* controls (**Fig. 1J,K** and **S1K**). As in previous *in vivo* assays, we also evaluated the frequencies of NSCs in both *Foxg1*-GOF

and -LOF cultures and used them to normalize the number of S100β$^+$ and Gfap$^+$ cells. [Here, NSCs were identified as expressing Sox2 but not an mCherry reporter under the control of the neuronogenic-lineage-specific *Tubulin-α1* promoter (**Fig. 1H,J**)]. Interestingly, we found that, at day in vitro (DIV) 4, NSCs were augmented by 89.64±10.67% (p<0.0001, n=4,4) in *Foxg1*-GOF cultures and decreased by 26.95% in *Foxg1*-LOF cultures (**Fig. 1I,K** and **S1F,J**). This implicates that the average, NSC-normalized astrocytic output varied by -80.96% (S100β$^+$ cells) and -52.41% (Gfap$^+$ cells) in *Foxg1*-GOF cultures, as well as by +32.93% (S100β$^+$ cells) in *Foxg1*-LOF cultures.

It is possible that what we observed in our assays did not depend on NSC fate choice, but it alternatively reflected an altered kinetic behaviour of astrocyte-committed progenitors originating from engineered NSCs. To fix this issue, we repeated the *in vitro Foxg1*-GOF assay adopting three *ad hoc* devices. First, we ran it over a shorter temporal window (four days for proliferation and two days for differentiation). Second, we took advantage of LIF stimulation to unmask early astroglial committed precursors. Third, we engineered both *Foxg1*-GOF and control preparations by lentiviruses harboring an additional *IRES-EGFP* module under pNes/TetON control, labelling NSCs and their immediate progenies, and we evaluated the Gfap$^+$EGFP$^+$/EGFP$^+$ ratio of each experimental preparation, as a more direct index of NSC-to-astroblast transition. Interestingly, we found that this ratio was diminished by 52.51±3.61% in *Foxg1*-GOF samples compared to controls (p<4.7*10^{-5}, n=4,4) (**Fig. 1L,M** and **S1L**), so confirming the negative impact exerted by *Foxg1* on the NSC astrogenic bias**.**

To secure this interpretation, we scored *Foxg1*-mutant NSCs by a classical clonal assay. Specifically, we made E11.5 cortico-cerebral precursors *Foxg1*-GOF or -LOF by dedicated lentiviral effectors, we kept them as floating neurospheres for four days, we let them attach on poly-D-lysinated coverslips at clonal density, and we evaluated their clonal outputs three days later (**Fig. 1N**). We observed a decrease of neuron-astrocyte-mixed clones in *Foxg1*-GOF assays (5.27±0.94% in mutants vs 25.45±1.24% in controls, p<10^{-5} n=4,4) and an increase of these clones in -LOF assays (32.83±2.33% in mutants vs 24.81±3.19% in controls, p<0.04, n=4,4). In case of *Foxg1*-GOF assays, we also found a decrease of astrocyte-only clones (1.38±0.48% in mutants vs 5.07±0.75% in controls, p<3.1*10^{-3}, n=4,4) as well as a concomitant increase of neuron-only clones (72.55±1.33% in mutants vs 60.56±2.14% in controls, p<1.6*10^{-3}, n=4,4) (**Fig. 1O,P** and **S1M,N**). Altogether, these data show that, in addition to stimulating NSC self-renewal, *Foxg1* antagonizes the NSC shift from neuronogenic towards astrogenic fates.

Finally, before investigating specific antiastrogenic mechanisms driven by *Foxg1*, we wondered about their general articulation, cell-autonomous or not cell-autonomous. As *Foxg1-GOF* precursors gave rise to reduced astroglial outputs upon their transplantion into *wild type* brains (**Fig. 1A,E**), we expected that cell-autonomous mechanisms should play a likely prevalent role in this context. To corroborate this inference and unveil possible, collateral non-autonomous processes, we repeated the test shown in Fig. H1,I, with some *ad hoc* modifications. Specifically, we monitored the histogenetic behaviour of aliquots of *sensor* (S) E12.5 wild type pallial precursors, acutely labelled by a constitutively expressed mCherry transgene, following their 1:4 co-

culture with isochronous *conditioner* (C) precursors, pre-made gain-of-function for *Foxg1* or a control (**Fig. 1Q**). It turned out that the ratio among $Gfap^{+}mCherry^{+}$ astrocytes and total $mCherry^{+}$ cells was not affected by the "genotype" of the co-cultured C-derivative population, while *Foxg1* overexpression by C-founders down-regulated the fraction of their descendants expressing Gfap (-19.44±2.69%, $p<2.3*10^{-3}$, n=6,5) (**Fig. 1R**). All that confirms that *Foxg1* inhibition of astrogenesis largely relies on cell-autonomous mechanisms and suggests that non-cell-autonomous processes hardly contribute to it.

***Foxg1* antagonizes the NSC astrogenic progression by downregulating key transcription factors channelling NSCs to astrogenic fates.**

We hypotesized that the anti-astrogenic activity of Foxg1 could primarily originate from its ability to down-regulate a small set of key transcription factor genes promoting the neuronogenic-vs-astrogenic switch: *Couptf1*, *Sox9*, *Nfia* and *Zbtb20* (Naka et al. 2008; Kang et al. 2012; Nagao et al. 2016). In fact, Foxg1 is a well known transcriptional inhibitor (Li et al. 1995; Yao et al. 2001). Moreover, as resulting from Jaspar analysis (Mathelier et al. 2014), *Couptf1*, *Sox9*, *Nfia* and *Zbtb20* loci harbor a number of putative Foxg1-binding sites, among which a few high-score, evolutionarily conserved ones (**Fig. S2A-D**). We tested this prediction in pre-gliogenic neocortical precursors made *Foxg1*-GOF by somatic lentiviral transgenesis (**Fig. 2A-C**; control-norm-[*Foxg1*-mRNA] = 4.42±0.64, not shown). As expected, all four genes resulted to be down-regulated upon *Foxg1* overexpression, by -41.5±7.01% ($p<0.045$, n=4,4), -30.98±5.05% ($p<0.046$, *n=6,6*), -55.85±4.73% ($p<0.003$, *n=6,6*), and -24.30±9.34% ($p<0.038$, *n=6,6*), respectively (**Fig. 2D,E**). No changes were conversely detectable in *Foxg1*-knockdown cultures (**Fig. 2B,C,F**; control-norm-[*Foxg1*-mRNA] = 0.65±0.04, not shown), suggesting that gene down-regulation observed in *Foxg1*-GOF preparations did not reflect a dominant-negative effect.

Then, to assess functional relevance of these phenomena to *Foxg1* anti-astrogenic activity, as a proof-of-principle, we overexpressed *Zbtb20* and *Nfia* in wild type (**Fig. S3A-C**) and *Foxg1*-overexpressing precursors and we evaluated the histogenetic outcome of these manipulations by dedicated clonal assays (**Fig. 2G**). While not fully rescuing the *Foxg1*-GOF phenotype, the transduction of a constitutively active *Zbtb20* transgene into *Foxg1*-GOF cultures mitigated the absolute frequency decrease of neuronal-astroglial and astroglial clones evoked by *Foxg1* overexpression compared to controls (from -25.37% to -13.11%, $p<0.009$, n=4,4, and from -7.51% to -4.55%, ($p<0.021$, n=4,4, respectively). [Here, control frequencies of neuronal-astroglial and astroglial clones were 36.23±2.14% and 8.89±1.70%, respectively]. On the other side, *Zbtb20* alone did not significantly alter the frequencies of the different clone types. This suggests that, rather than simply *compensating* for it, *Zbtb20* transduction *partially rescued* a key molecular event mediating *Foxg1* impact on NSC fate choice (**Fig. 2H** and **S4A**). As for *Nfia,* its overexpression in *Foxg1*-GOF NSCs fully restored the drop of mixed clones caused by *Foxg1* upregulation [these clones were as little as 5.63±0.48% in *Foxg1*-GOF cultures compared to 21.69±3.53% in controls ($p<0.002$, n=4,4)], while not affecting the prevalence of these clones if elicited in control NSCs. Moreover, *Nfia* also abolished the slight increase of neuronal clones (75.17±1.73% vs

69.49±2.43%, $p<0.049$, $n=4,4$) as well as the decrease of astroglial ones (1.24±0.46% vs 4.62±0.79%, $p<0.005$, $n=4,4$) caused by *Foxg1* overexpression. Remarkably, however, its overactivation in control NSCs almost halved the frequency of neuronal clones (40.19±2.03% vs 69.49±2.43%, $p<0.001$, $n=4,4$) and elicited a massive increase of astroglial ones (24.99±1.17% vs 4.62±0.79%, $p<0.001$, $n=4,4$) (**Fig. 2I** and **S4B**). All this indicates that, in addition to *rescuing* the *Foxg1*-GOF phenotype, the *Nfia* transgene also *overcompensated* for it.

Finally, to cast light on molecular mechanisms mediating *Foxg1*-driven downregulation of *Couptf1*, *Sox9*, *Nfia* and *Zbtb20*, we profiled chromatin of mid-neuronogenic neocortical precursors, both control and *Foxg1*-GOF, for Foxg1 recruitment at selected regions of the corresponding loci, by Chromatin Immuno-Precipitation (ChIP)-qPCR. (**Fig. 2J**). Specifically, nine Foxg1-BSs were inspected, 2 for *Couptf1*, 3 for *Zbtb20*, 2 for *Sox9* and 2 for *Nfia*. These BSs included four putative ones selected by Jaspar software (Mathelier et al. 2014), with score index above 14 ($^{[J14]}$Foxg1-BSs), and shared by mice and humans, as well five experimentally verified ones, reported by the NCBI-GEO database ($^{[EXP]}$Foxg1-BSs) (**Fig. S2A-D**). In general, all these BSs were specifically enriched in αFoxg1-immuno-precipitates compared to IgG-treated samples (however this does not apply to *Couptf1*-Foxg1-BS.h1 and *Nfia1*-Foxg1-BS.h1 in control αFoxg1-immuno-precipitates) (**Fig. 2K**). Interestingly, in case of *Couptf1*, *Sox9* and *Nfia* loci, there was at least one BS significantly over-enriched in *Foxg1*-GOF compared to control αFoxg1-immuno-precipitates [BSs displaying *Foxg1*-responsive enrichment included: *Couptf1*-Foxg1-BS.h1 (3.83±0.43% vs 1.60±0.24%, $p<0.005$, $n=4,3$), *Couptf1*-Foxg1-BS.a (1.36±0.15% vs 0.88±0.19%, $p<0.050$, $n=4,4$), *Sox9*-Foxg1-BS.h1 (2.02±0.25% vs 1.25±0.26%, $p<0.025$, $n=4,3$) and *Nf1a*-Foxg1-BS.h1 (4.56±0.47% vs 2.66±0.41%, $p<0.017$, $n=4,3$)] (**Fig. 2K**). All this suggests that Foxg1 directly trans-represses *Couptf1*, *Sox9*, *Nfia* and *Zbtb20,* and that such trans-repression may contribute to the decline of *Couptf1*, *Sox9 and Nfia* transcripts occurring in *Foxg1*-GOF precursors.

Foxg1 antagonizes astrogenesis by directly transrepressing astroglial genes.

We hypothesized that *Foxg1* inhibition of astrogenesis could be further strenghtened by a direct impact of Foxg1 on genes implementing the astroglial differentiation program. To assess this issue, first we investigated the response of selected astroglial genes, *Gfap, S100β* and *Aqp4,* to *Foxg1* manipulation. For this purpose, we employed E14.5 cortico-cerebral precursors engineered for TetON-controlled *Foxg1* overexpression, kept in the presence of growth factors and terminally pulsed by LIF (**Fig. 3A**). As expected, we found that *Gfap-, S100β- and Aqp4*-mRNA levels were significantly decreased, by -49.92±13.25% ($p<0.03$, $n=6,6$), -46.79±16.91% ($p<0.03$, $n=5,5$), and -43.98±14.70% ($p<0.03$, $n=5,5$), respectively (**Fig. 3B**, left). No statistically significant changes of these mRNAs were observed in a specular *Foxg1*-LOF assay (**Fig. 3B**, right), so ruling out any dominant negative effects.

Next, to cast light on mechanisms mediating *Foxg1*-dependent repression of these genes, we selected a set of putative Foxg1-binding sites (BSs) within *Gfap, S100β* and *Aqp4* promoters (2 for *Gfap*, 3 for *S100β* and 2

for *Aqp4*), by Jaspar software (Mathelier et al. 2014) (**Fig. S2E-G**). Then, we monitored the actual recruitment of Foxg1 to these sites, both in control and *Foxg1*-GOF cells, by ChIP-qPCR. To this aim, we employed chromatin extracted from derivatives of E12.5 cortico-cerebral precursors, processed as in **Fig. 3C**. We found that the chromatine enrichment elicited by αFoxg1 ranged from 0.63±0.17% (*Aqp4*_Foxg1-BS.a, *n*=4,4) to 3.36±1.87% (*S100β*_Foxg1-BS.a, *n*=4,4) in control samples, well above the background ChIP signal given by control IgG. Moreover, such enrichment did not generally change in *Foxg1*-GOF samples, suggesting that Foxg1 binds to these sites with high affinity. In the only case of *Gfap*_Foxg1-BS.b, this enrichment – about 1.36±0.32% in controls – arose up to 2.29±0.12% upon *Foxg1* overexpression ($p<1.7*10^{-3}$, *n*=4,4) (**Fig. 3D**). This means that this interaction could contribute to differential regulation of *Gfap* in *Foxg1*-GOF samples.

Foxg1 antagonizes astrogenesis via a pleiotropic impact on key pathways tuning astroglial genes.

In addition to its direct effect on astroglial genes, we hypothesized that *Foxg1* might further dampen their activity indirectly, by impacting trans-active modulators of their transcription. In particular, we focused our attention on four key pathways involved in fundamental control of astroglial gene transcription: IL6/Jak2/Stat1,3; Bmp/Smad1,5,8; Nrg1/ErbB4^{ICD}-NCoR; Dll1/Notch1^{ICD}. For these pathways, we measured nuclear levels of their ultimate nuclear effectors (modulating gene transcription) within *Foxg1*-GOF, Nestin^{+} NSCs. We also evaluated nuclear NSC levels of a key antagonist of the IL6/Jak2/Stat1,3 pathway, Neurog1. We acutely engineered E12.5 corticocerebral precursors, making them to overexpress *Foxg1* in the neurostem compartment. We kept these precursors in culture under growth factors for seven days, and we finally co-immunoprofiled them for Nestin and the six effectors in order, each evaluated by quantitative immunofluorescence (qIF): p[Tyr^{705}]Stat3, p[Ser$^{463/465}$]Smad1,5,8, Neurog1, ErbB4^{ICD}, NCoR1, and Notch1^{ICD} (**Fig. 3E**). We found that p[Tyr^{705}]Stat3, p[Ser$^{463/465}$]Smad1,5,8, and Notch1^{ICD} were downregulated, by -58.28±1.99% ($p<2.5x10^{-10}$, *n*=300,310), -52.91±2.34% ($p<5.8x10^{-23}$, *n*=270,220), and -13.78±1.20% ($p<2.7x10^{-7}$, *n*=207,404), respectively. ErbB4^{ICD} was unaffected. Conversely, Neurog1 and NCoR1 were slightly, albeit significantly upregulated, by +8.75±3.56% ($p<0.032$, *n*=182,150) and +14.18±2.83% ($p<0.0002$, *n*=212,281), respectively (**Fig. 3G** and **S4C-H**).

To address the relevance of such changes to astrogenesis inhibition, we functionally counteracted them by transducing E12.5 neocortical precursors, made acutely *Foxg1*-GOF, with pre-validated (**Fig. S3D-G**), "rescuing" Xi lentiviruses. We kept engineered cells as proliferating neurospheres for seven days under growth factors. We allowed them to differentiate for four more days. Finally, we evaluated their S100β^{+} astroglial output (**Fig. 3F**). We found that constitutively active Stat3 (caStat3) (Hillion et al. 2008) lessened the astroglial deficit elicited by *Foxg1* overexpression, however only to a limited extent (normalized against controls, this deficit moved from -66.46±3.15% to -49.70±6.29%, $p<0.03$, *n*=4,4). Conversely, constitutively active Smad1 (Fuentealba et al. 2007) (caSmad1), alone or in combination with caStat3, fully restored the normal astroglial output. In a similar way, functional NCoR1 inhibition, via knock down of its necessary Tab2 cofactor (Sardi et

al. 2006), considerably reduced the *Foxg1*-dependent astrogenic deficit (**Fig. 3H** and **S6A-D**). Remarkably, in all these cases the delivery of the "rescuing agent" to *control* cultures did not upregulate astrogenesis rates [*caStat3* and *caSmad1* reduced the output of these cultures (**Fig. 3H)**, possibly because of premature shrinkage of their neurostem compartment (**Fig. S5A**)]. All this suggests that each of these agents did not simply *mask* the astrogenic deficit elicited by *Foxg1* overexpression, via compensatory mechanisms independent from *Foxg1* regulation. It rather indicates that they *abolished* molecular abnormalities which specifically mediate the impact of *Foxg1* overexpression on astrogenesis. Last, NSC transduction of a constitutively active $Notch^{ICD}$ transgene (Cassady et al. 2014) failed to rescue the hypo-astrogenic *Foxg1*-GOF phenotype. Moreover, it *reduced* the $Gfap^{+}$ astroglial output of both control and *Foxg1*-GOF cultures, from 100±8.35% to 21.64±2.48% (control-normalized frequencies, $p<0.001$, $n=4,4$), and from 40.28±5.63% to 26.34±4.71% (control-normalized frequencies, $p<0.001$, $n=4,4$), respectively (**Fig. 3H** and **S6E**). This phenomenon was unexpected. It likely reflected the defective capability of derivatives of $Notch^{ICD}$-overepressing NSCs to respond to astrogenic cytokines and activate the mature astroglial marker Gfap (**Fig. S5B**).

Next, we investigated basic mechanisms leading to pStat3 and pSmad1,5,8 deficits. We evaluated the impact of *Foxg1* manipulations on key players implicated in the corresponding signalling machineries (**Fig. 4A**). As for the IL6/Jak2/Stat1,3 axis, we found a significant downregulation of *Gp130-, Jak2-* and *Stat3*-mRNAs (*Gp130:* -24.51±6.53%, $p<0.05$, $n=6,6$; *Jak2:* -54.33±6.52%, $p<0.0002$, $n=6,6$; *Stat3:* -32.26±8.88%, $p<0.03$, $n=6,6$) and no changes for *Il6Ra*-mRNA in *Foxg1*-GOF cultures (**Fig. 4B**). *Jak2*- and *Stat3*-mRNA were conversely upregulated in *Foxg1*-LOF cultures (*Jak2:* +13.32±3.80%, $p<0.02$, $n=6.6$; *Stat3:* +10.59±2.44%, $p<0.02$, $n=6.6$), whereas *Gp130*- and *Il6Ra*-RNA were unaffected (**Fig. 4C**). Concerning the Bmp/Smad1,5,8 pathway, *BmpRII*-mRNA was downregulated in *Foxg1*-GOF samples (-29.59±11.44%, $p<0.03$, $n=6.6$) (**Fig. 4B**) and unaffected in *Foxg1*-LOF ones (**Fig. 4C**). *Bmp4* was not affected at all. Last, *NCoR1*-mRNA levels, implicated in the balance between $Notch^{ICD}$ and $ErbB4^{ICD}$-mediated signalling, did not show any significant change either in *Foxg1*-GOF and -LOF cultures (**Fig. 4B,C**). Finally, as a proof-of-principle, to assess relevance of the changes described above to the *Foxg1*-GOF astroglial phenotype, we counteracted the *Jak2*-mRNA decline peculiar to *Foxg1*-GOF neocortical precursors by a lentiviral expressor encoding for the constitutively active, $JAK2^{V617F}$ mutant kinase (Vainchenker 2005), and we evaluated the impact of this manipulation on $Gfap^{+}$ cell frequency (**Fig. 4D**). Interestingy, the introduction of a $JAK2^{V617F}$ transgene in *Foxg1*-GOF cultures mitigated the decline of $Gfap^{+}$ cells caused by *Foxg1* overexpression, which moved from -43.13±4.02% to -30.26±2.84% (control-normalized frequencies, $p<0.020$, $n=4,4$). The frequency of these cells was conversely unaffected, when $JAK2^{V617F}$ was delivered to controls (**Fig. 4E** and **S6F**). All this suggests that the downregulation of *Jak2* (and, possibly, other *Foxg1*-sensitive, IL6/Jak2/Stat1,3- and Bmp/Smad1,5,8- signaling mediators reported above) may contribute to *Foxg1* inhibition of astroglial genes expression.

Foxg1 impairs transactivating abilities of the pStat3-pSmad1,5,8 complex.

It was previously shown that Foxg1 chelates Smad1 and Smad4 (Rodriguez et al. 2001). Therefore, we wondered if it may antagonize astrogenesis, by impairing intrinsic transactivating abilities of these Bmp signalling effectors. To address this issue, we acutely engineered E12.5 neocortical precursors with two transgenes, encoding for constitutively active Stat3 (caStat3) and Smad1 (caSmad1), driven by a constitutive promoter (*Pgk1-p*). To sense the activity of the resulting caStat3-caSmad1 complex in a way independent of possible local epigenetic effects of Foxg1 on astroglial gene chromatin, we employed a synthetic Bmp-signalling sensor (*BmpRE-ZsGreen*), delivered via a randomly integrating lentivector. To so-engineered neural cells, we concomitantly delivered a *Foxg1*-expressing lentivirus or a control. We kept these cells for ten days in pro-proliferative conditions and, lastly, we profiled them for EGFP fluorescence by cytofluorimetry (**Fig. 4F**). We found that both the frequency of ZsGreen^{+} cells and the median fluorescence intensity of ZsGreen^{+} cells were reduced in *Foxg1*-GOF samples, by 38.38±6.63% (control-normalized value, $p<0.05$, $n=4,4$), and 26.88±2.78% (control-normalized value, $p<0.001$, $n=4,4$), respectively (**Fig. 4G**). Conversely, in a parallel control assay where the *BmpRE-ZsGreen* Bmp-signalling sensor was replaced by a *pPgk1-mCherry* transgene, no *mCherry* expression decline was detectable in *Foxg1*-GOF samples (not shown). These results suggest that Foxg1 may dampen the intrinsic, pSmad1/4 transactivating power.

***Foxg1* NSC expression levels progressively decline before the perinatal astrogenic burst.**

We wondered if *Foxg1* anti-astrogenic activity might be instrumental in the proper temporal progression of astrogenesis. Specifically, we hypothesized that high *Foxg1* levels in early NSCs could refrain them from differentiating to astroblasts, while lower levels peculiar to later NSCs could be permissive to such differentiation. To address this issue, we measured *Foxg1*-mRNA and -protein levels within pallial stem cells of different ages.

In a first assay, we employed derivatives of E11.5 pallial precursors, cultured in pro-proliferative medium for 2 up to 7 days. From these cultures we FACsorted samples of NSCs (identified as pNes-EGFP^{+}pTα1-mCherry^{-}, upon lentiviral transduction of these reporters) at DIV2 and DIV7, approximately corresponding to *in vivo* E13.5 and E18.5, respectively. We analyzed their RNA and we found a significant decrease of *Foxg1*-mRNA level in DIV7 compared to DIV2 samples (-59.47±5.11%, $p<0.01$, $n=5,5$). Here, as controls, we also measured expression of *Zbtb20* and *Neurog1*, two genes active in NSCs according to opposite temporal progressions (Hirabayashi et al. 2009; Ohtsuka et al. 2011). As expected, *Zbtb20* and *Neurog1* were increased and decreased, respectively, in more aged samples (**Fig. 5A,B**). In a second assay, we evaluated Foxg1 protein level in DIV2 and DIV6 Nestin^{+} NSC derivatives of E12.5 acutely dissociated neocortices, by double αNestin-αFoxg1 qIF. Compared to DIV2 samples, Foxg1 level was diminished by 52.55±1.47% at DIV6 ($p<3.6*10^{-10}$, $n=288,229$) (**Fig. 5C,D**), confirming that a robust Foxg1 expression decline occurs in neocortical stem cells concomitantly with the neuronogenic-to-astrogenic transition.

To corroborate these findings, we compared *in vivo* Foxg1 expression at late vs early neuronogenic stages of neocortical development. As expected, we found that periventricular Foxg1 levels overtly declined at E16.5 with respect to E12.5 (**Fig. 5F**). Consistently, qIF profiling of acutely dissociated neocortices showed that a -27.19±1.2% Foxg1 decline ($p<8.18*10^{-40}$, n=407,278) specifically occurred in E16.5 Nestin$^+$ NSCs compared to E12.5 ones (**Fig. 5G,H**). In other words the Foxg1 decline *preceded* the transition from neuronogenesis to astrogenesis, suggesting it could be instrumental in arousal of the latter.

***Foxg1* antiastrogenic activity is conserved in human pallial precursors.**

To assess if *FOXG1* antagonizes astrogenesis progression in humans like in rodents, we run an *ad hoc* GOF assay in late pallial precursors derived from a legal, human PCW10 abortion, pre-expanded in vitro over about 150 days. At the beginning of the procedure (DIV 0), we transduced these precursors with two lentiviruses, expressing the rtTA^{M2} transactivator under the constitutive *Pgk1* promoter and *Foxg1* (or a control) under the rtTA^{M2}/doxycycline-responsive TREt promoter (**Fig. 6A**). We kept the engineered cells for 7 days in proliferation medium and 7 more days in differentiation medium. We exposed them to 9ng/ml doxycyclin from DIV0 to DIV11 (so eliciting a final expression gain about 4, not shown) and we immunoprofiled their derivatives at DIV15 for S100β (which is mainly confined to cells expressing the pan-astrocytic marker AldoC in these cultures; not shown). It turned out that S100β$^+$ astrocyte frequency was reduced by -51.29±8.05% in *Foxg1*-GOF samples compared to controls ($p<0.006$, n=4,4) (**Fig. 6A** and **S7A**). To get a closer insight into *FOXG1* role in human NSC fate choice, we run an additional GOF assay, differing from the previous one in three aspects. We restricted *Foxg1* overexpression to the NSC compartment, under the control of the *pNes* promoter; we shortened the differentiation phase of the procedure by 4 days; we exposed the engineered cells to a terminal, 24h pulse of LIF. Then, we evaluated the frequency of cells expressing GFAP (specifically detectable in astroglial, but also neurostem human cells (Malatesta et al. 2008)) as a proxy of the NSC astrogenic bias (**Fig. 6B**). Immunoprofiling of these cultures at DIV10 showed that such frequency was reduced by -27.66±5.41% in *Foxg1*-GOF samples compared to controls ($p<0.003$, n=4,4) (**Fig. 6B** and **S7B**). All this supports the hypothesis that *Foxg1* may antagonize the NSC astrogenic progression in humans like in rodents.

Next, to corroborate these results and rule out that they originated from a dominant negative effect, we interrogated a sister preparation of the PCW10 neocortical precursors referred to above, pre-expanded in vitro over about 120 days, by a NSC-restricted *FOXG1*-LOF approach (**Fig. 6C** and **S7C**). For this purpose, we transduced such precursors by a lentiviral mix encoding for *pNes*-driven expression of miR.αFoxg1.1690 (this is an RNAi effector decreasing *FOXG1*-mRNA levels by about 42% upon constitutive, *Pgk1p*-driven expression in mixed neural cultures; data not shown). Then, we kept transduced cells 7 days in proliferative medium and 3 more days in a differentiative medium, terminally supplemented by Lif. Finally, we immunoprofiled cells for neurostem/astroglial markers. Frequency of Egfp$^-$GFAP$^+$ astrocytes was unaffected. Conversely, normalized against controls, Egfp$^+$GFAP$^\pm$ NSCs were reduced by -26.97±7.82% ($p<0.025$, n=3,3). All this points to a robust

increase of the NSC-normalized GFAP$^+$ astroglial output (normalized against controls, +58.59±3.83%, p<0.003, n=3,3) (**Fig. 6C)**. It further suggests that the negative *FOXG1* impact on NSC astrogenic progression emerging from overepression assays is a genuine GOF phenotype.

Last, to assess a possible conservation of mechanisms mediating *Foxg1* impact on astrogenesis progression, we downregulated *FOXG1* in human, PCW10+DIV120 neocortical precursors by a constitutively expressed RNAi effector (*αFoxg1*-shRNA) and monitored the impact of this manipulation on human orthologs of murine mediators of this activity (**Fig. 6D)**. We found that, upon a -22.19±3.73% decline of *FOXG1*-mRNA (p<0.049, n=3,3), *ZBTB20*-mRNA was upregulated by +26.48±2.72% (p<0.005, n=3,3), and *COUPTF1*, *SOX9* and *NFIA* were unaffected. Moreover, mRNAs of *Egfp* and *ZsGreen* reporters, driven by pStat1,3- and Bmp-responsive elements (REs) and co-delivered to neural cells by dedicated lentivectors with a *Pgk1p*-driven *mCherry* normalizer, were also robustly upregulated, by +252.55±105.72% (p<0.025, n=3,2) and +168.81±71.90% (p<0.050, n=3,3), respectively (**Fig. 6D)**. All that suggest that key molecular mechanisms mediating *Foxg1* control of astrogenesis are shared by placental mammals.

DISCUSSION

In this study we showed that *Foxg1* overexpression within murine neocortical stem cells antagonizes the generation of astrocytes, *in vivo* as well as *in vitro*, while stimulating NSC self-renewal and promoting neuronogenesis (**Fig. 1**). We discovered that *Foxg1* antiastrogenic activity can originate from four concurrent mechanisms. Foxg1 trans-represses key transcription factor genes promoting the NSC-to-astrocyte progenitor progression (**Fig. 2**). It also directly trans-represses astroglial genes, i.e. genes implementing the astroglial differentiation program (**Fig. 3A-D**). Next, it tunes multiple key pathways controlling astroglial gene transcription, unbalancing nuclear concentration of their ultimate effectors (pStat3, pSmad1,5,8, NCoR1, Notch^{ICD}) and so further dampening astroglial gene expression (**Fig. 3E-H** and **4A-E**). Last, it jeopardizes trans-activating abilities of one of these effectors, the pStat3-pSmad1,5,8 complex (**Fig. 4F,G**). Moreover, we found that Foxg1 levels within neocortical NSCs progressively decline *prior to* the neuronogenic-to-gliogenic transition (**Fig. 5)**, suggesting an involvement of Foxg1 in fine temporal tuning of astrogenesis rates. Finally, we provided a proof-of-principle that a similar anti-astrogenic activity is played by Foxg1 in *human* neocortical precursors (**Fig. 6**), pointing to such activity as an evolutionarily conserved trait.

Interestingly, a robust *Foxg1*-dependent inhibition of astrogenesis was observed *in vivo*, upon a variety of functional assays (**Fig. 1A-G**). In particular, a shrinkage of the astroglial output occurred only when *Foxg1* was upregulated (**Fig. 1E,G** and **6A-C**), ruling out any artifactual dominant negative effect. Furthermore, after normalization of such output against the starting size of the NSC compartment (**Fig. 1E,F** and **6A-C**), *Foxg1* capability to inhibit astrogenesis emerged upon both gain- and loss-of-function approaches, suggesting that this process is sensitive to even subtle changes of Foxg1 levels around baseline. Noticeably, these observations were

performed upon transplantation of neural precursors pre-manipulated *in vitro* by lentiviral transgenesis, an approach allowing for stable and accurate control of gene expression levels.

Next, the astrogenesis decline evoked by *Foxg1* overexpression in NSCs was not simply due to a general differentiation deficit of neocortical precursors. In fact, it was associated to a pronounced, *absolute* increase of neuronogenesis (**Fig. 1H,I**). As emerging from clonal assays (**Fig. 1N-P**), this did reflect a net, consistent shift in the NSC histogenetic choice. This means that channelling NSCs towards neuronal rather than glial fates is a genuine, key role exerted by Foxg1 in normal development.

Last, an anti-astrogenic activity was observed when NSC-restricted *Foxg1* overexpression was switched on *in vivo*, in a late-neuronogenic, *isochronic* environment (**Fig. 1C,G**). Moreover, clone founder cells showed an altered astrogenic bias following *Foxg1* manipulation *during the neuronogenic phase* (**Fig. 1N-P**). Not least, *Foxg1* NSC levels (both mRNA and protein) turned out to progressively decline, while moving from early neuronogenic stages to subsequent gliogenic phases (**Fig. 5**). All this suggests that a progressive decline of Foxg1 levels is among key factors dictating age-dependent, NSC developmental choices (Ohtsuka et al. 2011; Okamoto et al. 2016).

As for *cellular* articulation of *Foxg1* activity, it has to be emphasized that astrogenesis inhibition was detectable upon *NSC-restricted Foxg1* overexpression (**Fig. 1A,C,D,H,N** and **6B**), by scoring progenies of engineered neural precursors transplanted in wild type brains (**Fig. 1E,G**) or allowed to differentiate *in vitro* (**Fig. 1I,O** and **6B**). It is known that, despite the relevance of environmental signals to the progression of early pallial precursors towards gliogenesis (Morrow et al. 2001), such progression can largely occur in a clone-autonomous way (Qian et al. 2000). Our data indicate that *Foxg1* largely acts via cell-autonomous mechanisms and contributes to intra-clonal astrogenesis control (**Fig. 1Q,R**).

Concerning *molecular* articulation of *Foxg1* activity, this was quite complex. Foxg1 targets included genes involved in both *choice* and *implementation* of the astrogenic program. Moreover its impact on these targets was direct as well as indirect (**Fig. 7**).

First of all, Foxg1 down-regulated selected transcription factor genes which normally *promote NSC acquisition of astrogenic competence* (**Fig. 2A-F**). These were: *Zbtb20* and its *Couptf1* target, stimulating the histogenetic progression of neocortical precursors and specifically increasing their responsivity to astrogenic cytokines (Naka et al. 2008; Nagao et al. 2016; Tonchev et al. 2016), as well as *Sox9* and its *Nfia* target, both promoting the respiration increase associated to the NSC-to-astrocyte progenitor transition (Kang et al. 2012), the latter sustaining astroglial gene promoter demethylation (Namihira et al. 2009). Apparently, all four genes were *directly* trans-repressed by Foxg1 (**Fig. 2J,K**). However, indirect mechanisms also likely contributed to their dynamics. For example, the drop of *Sox9*-mRNA might have been exacerbated by the *Foxg1*-dependent collapse of the IL6/Jak2/Stat3 pathway, which normally sustains its expression (Hall et al. 2017; Jeselsohn et al. 2017). In a similar way, the decrease of *Nfia*-mRNA might reflect the downregulation of both *Sox9*, acting

upstream of it (Kang et al. 2012), and nuclear Notch^{ICD}, also promoting its transcription (Namihira et al. 2009). Conversely, *Zbtb20,* insensitive to caStat3, Bmp4, Notch^{ICD}, Sox9 or Nfia (Nagao et al. 2016), might have been suppressed by Foxg1 via prevalently direct mechanisms. Intriguingly, *Zbtb20* and *Foxg1* play contrasting roles in other key neuro-developmental scenarios too, e.g. in medial-lateral pallial specification, as promoters of archicortical and neocortical fates, respectively (Muzio and Mallamaci 2005; Nielsen et al. 2007, 2010).

Next, Foxg1 further repressed genes which *implement the astroglial program within committed progenitors and their mature progenies*, such as *Gfap*, *S100b*, *Aqp4* (**Fig. 3A,B**). Even in this cases, gene down-regulation was likely mediated by direct (**Fig. 3C,D**) as well as indirect (**Fig. 3E-H**) mechanisms.

Among the most prominent molecular changes underlying *Gfap* downregulation, there was the pronounced pSmad1,5,8 decrease evoked by Foxg1 overexpression in NSCs (**Fig. 3F,G**), possibly as a consequence of reduced sensitivity of these cells to Bmp ligands (**Fig. 4A,B**). Moreover Foxg1 apparently jeopardized the transactivating abilities of the "active Smad1-active Stat3"-containing complex (**Fig. 4F,G**), likely by chelating Smad1, as already described in heterologous systems (Rodriguez et al. 2001). However, the Smad1,5,8 machinery is limiting to both neuronogenesis and astrogenesis progression (Nakashima 1999; Sun et al. 2001; Hirabayashi et al. 2009). Therefore, a Bmp signalling decrease should be able to simply *exacerbate* the absolute astrogenic deficit evoked by *Foxg1*, not *cause* it. We propose that this deficit primarily stem from the collapse of pStat3 (**Fig. 3F,G**), in the presence of sustained Neurog1 expression (**Fig. 3G**). The former was reasonably due to the down-regulation of at least three key components of the corresponding signalling cascade (**Fig. 4A,B**). The latter, at odds with *Foxg1*-dependent upregulation of the canonical *Neurog1* inhibitor, *Hes1* (Chiola et al. in press; Cau et al. 2000; Brancaccio et al. 2010), was perhaps promoted by *Foxg1* via *Pax6* (Blader 2004; Manuel et al. 2010). Regardless of mechanisms unbalancing their levels, both pStat1 and Neurog1 are known to compete for limited p300 and pSmad1 cofactors available, to form an active trimer which transactivates astroglial or neuronal genes, respectively (Nakashima 1999; Sun et al. 2001). In this way, in the presence of reduced pSmad1 levels, even a moderate decline of the pStat1/Neurog1 ratio may have a truly disruptive effect on astroglial genes activation.

In a similar way, even the subtle changes of nuclear NCoR1 and Notch^{ICD} evoked by Foxg1 (**Fig. 3G**) might significantly concur to defective astrogenic performances of *Foxg1*-GOF NSCs. In fact, both these factors compete for the same RBPJk bridge (Kao et al. 1998), mediating their interaction with astroglial genes (Ge et al. 2002; Hermanson et al. 2002). In this way, the increase of the NCoR1/Notch^{ICD} ratio occurring in *Foxg1*-GOF NSC nuclei ((114.18/86.22-1)*100% = +32.42%, see **Fig. 3G**) might severely unbalance this competition, so resulting in prevailing inhibitory, RBPJk-mediated inputs to astroglial promoters. To note, the moderate upregulation of nuclear NCoR1 occurring in *Foxg1*-GOF samples (**Fig. 3G**), not due to *NCoR1* gene transactivation (**Fig. 4A,B**), could reflect the decline of the IL6/Jak2/Stat3 cascade, instrumental in its nucleus-to-cytoplasm translocation (Sardi et al. 2006). As for Notch^{ICD}, we largely ignore mechanisms underlying its

dynamics. Moreover, the apparently negative impact of its overexpression on the astroglial output (**Fig. 3G** and **S5B**) deserves further investigations.

Last, *Foxg1* regulation of astrogenesis is not peculiar to rodents. In fact, we found that similar phenomena can be detected when *Foxg1* expression levels are manipulated in *human* pallial precursors. In this respect, it has been shown that an abnormal *FOXG1* copy number results in severe neurological pathologies, such as a variant of Rett syndrome, linked to *FOXG1* haploinsufficiency (Guerrini and Parrini 2012), and a variant of West syndrome, associated to *FOXG1* duplication (Pontrelli et al. 2014). It is tempting to speculate that an alteration of astrogenesis profiles may take place in these patients and concur to their neurological symptoms.

In synthesis, we have found that *Foxg1* antagonizes astrogenesis in the developing rodent neocortex. We have disentangled a large body of molecular mechanisms mediating this activity. We have shown that *Foxg1* may contribute to proper temporal articulation of the NSC histogenetic bias. Finally, we have provided a proof-of-principle that *Foxg1* regulation of astrogenesis can be an evolutionary conserved trait, shared by different mammals.

ACKNOWLEDGEMENTS

We thank Nika Blecich who contributed to early setup of *in vitro* histogenetic assays. We are grateful to Marco Bestagno and Nicoletta Caronni for technical assistance in FACsorting procedures, as well as to Alberto Tommasini for supporting us with analytic cytofluorimetric assays.

This work was funded by Telethon Agency (grant GGP13034 to AM) and SISSA (intramurary funding to AM).

COMPETING INTERESTS

The authors declare no competing interests.

AUTHORS' CONTRIBUTIONS

CF dissected Foxg1 functions in murine neocortical precursors, analyzed the results and co-wrote the manuscript, MS contributed to dissect Foxg1 functions in murine and human neocortical precursors, GL and NC contributed to assays with murine precursors, GC performed initial experiments with human precursors, AV took care of cytofluorometry, LPJ and SP provided human neocortical precursors, AM designed the study, analyzed the results and wrote the paper.

REFERENCES

Barnabé-Heider F, Wasylnka JA, Fernandes KJL, Porsche C, Sendtner M, Kaplan DR, Miller FD. 2005. Evidence that embryonic neurons regulate the onset of cortical gliogenesis via cardiotrophin-1. Neuron. 48:253–265.

Blader P. 2004. Conserved and acquired features of neurogenin1 regulation. Development. 131:5627–5637.

Brancaccio M, Pivetta C, Granzotto M, Filippis C, Mallamaci A. 2010. Emx2 and Foxg1 inhibit gliogenesis and promote neuronogenesis. Stem Cells Dayt Ohio. 28:1206–1218.

Cassady JP, D'Alessio AC, Sarkar S, Dani VS, Fan ZP, Ganz K, Roessler R, Sur M, Young RA, Jaenisch R. 2014. Direct Lineage Conversion of Adult Mouse Liver Cells and B Lymphocytes to Neural Stem Cells. Stem Cell Rep. 3:948–956.

Cau E, Gradwohl G, Casarosa S, Kageyama R, Guillemot F. 2000. Hes genes regulate sequential stages of neurogenesis in the olfactory epithelium. Dev Camb Engl. 127:2323–2332.

Chiola S, Do MD, Centrone L, Mallamaci A. in press. Foxg1 overexpression in neocortical pyramids stimulates dendrite elongation via Hes1 and pCreb1 upregulation. Cereb Cortex.

Costa MR, Bucholz O, Schroeder T, Götz M. 2009. Late Origin of Glia-Restricted Progenitors in the Developing Mouse Cerebral Cortex. Cereb Cortex. 19:i135–i143.

Deloulme JC, Raponi E, Gentil BJ, Bertacchi N, Marks A, Labourdette G, Baudier J. 2004. Nuclear expression of S100B in oligodendrocyte progenitor cells correlates with differentiation toward the oligodendroglial lineage and modulates oligodendrocytes maturation. Mol Cell Neurosci. 27:453–465.

Derouet D, Rousseau F, Alfonsi F, Froger J, Hermann J, Barbier F, Perret D, Diveu C, Guillet C, Preisser L, Dumont A, Barbado M, Morel A, deLapeyrière O, Gascan H, Chevalier S. 2004. Neuropoietin, a new IL-6-related cytokine signaling through the ciliary neurotrophic factor receptor. Proc Natl Acad Sci U S A. 101:4827–4832.

Falcone C, Filippis C, Granzotto M, Mallamaci A. 2015. Emx2 expression levels in NSCs modulate astrogenesis rates by regulating EgfR and Fgf9. Glia. 63:412–422.

Fuentealba LC, Eivers E, Ikeda A, Hurtado C, Kuroda H, Pera EM, De Robertis EM. 2007. Integrating Patterning Signals: Wnt/GSK3 Regulates the Duration of the BMP/Smad1 Signal. Cell. 131:980–993.

Ge W, Martinowich K, Wu X, He F, Miyamoto A, Fan G, Weinmaster G, Sun YE. 2002. Notch signaling promotes astrogliogenesis via direct CSL-mediated glial gene activation. J Neurosci Res. 69:848–860.

Ge W-P, Miyawaki A, Gage FH, Jan YN, Jan LY. 2012. Local generation of glia is a major astrocyte source in postnatal cortex. Nature. 484:376–380.

Gorski JA, Talley T, Qiu M, Puelles L, Rubenstein JLR, Jones KR. 2002. Cortical excitatory neurons and glia, but not GABAergic neurons, are produced in the Emx1-expressing lineage. J Neurosci Off J Soc Neurosci. 22:6309–6314.

Guerrini R, Parrini E. 2012. Epilepsy in Rett syndrome, and *CDKL5* - and *FOXG1* -gene-related encephalopathies: *MECP2-CDKL5-FOXG1- Related Encephalopathies*. Epilepsia. 53:2067–2078.

Hall MD, Murray CA, Valdez MJ, Perantoni AO. 2017. Mesoderm-specific Stat3 deletion affects expression of Sox9 yielding Sox9-dependent phenotypes. PLOS Genet. 13:e1006610.

Hanashima C, Fernandes M, Hebert JM, Fishell G. 2007. The role of Foxg1 and dorsal midline signaling in the generation of Cajal-Retzius subtypes. J Neurosci. 27:11103–11111.

He F, Ge W, Martinowich K, Becker-Catania S, Coskun V, Zhu W, Wu H, Castro D, Guillemot F, Fan G, de Vellis J, Sun YE. 2005. A positive autoregulatory loop of Jak-STAT signaling controls the onset of astrogliogenesis. Nat Neurosci. 8:616–625.

Hébert JM, McConnell SK. 2000. Targeting of cre to the Foxg1 (BF-1) Locus Mediates loxP Recombination in the Telencephalon and Other Developing Head Structures. Dev Biol. 222:296–306.

Hermanson O, Jepsen K, Rosenfeld MG. 2002. N-CoR controls differentiation of neural stem cells into astrocytes. Nature. 419:934–939.

Hillion J, Dhara S, Sumter TF, Mukherjee M, Di Cello F, Belton A, Turkson J, Jaganathan S, Cheng L, Ye Z, Jove R, Aplan P, Lin Y-W, Wertzler K, Reeves R, Elbahlouh O, Kowalski J, Bhattacharya R, Resar LMS. 2008. The High-Mobility Group A1a/Signal Transducer and Activator of Transcription-3 Axis: An Achilles Heel for Hematopoietic Malignancies? Cancer Res. 68:10121–10127.

Hirabayashi Y, Suzki N, Tsuboi M, Endo TA, Toyoda T, Shinga J, Koseki H, Vidal M, Gotoh Y. 2009. Polycomb Limits the Neurogenic Competence of Neural Precursor Cells to Promote Astrogenic Fate Transition. Neuron. 63:600–613.

Jeselsohn R, Cornwell M, Pun M, Buchwalter G, Nguyen M, Bango C, Huang Y, Kuang Y, Paweletz C, Fu X, Nardone A, De Angelis C, Detre S, Dodson A, Mohammed H, Carroll JS, Bowden M, Rao P, Long HW, Li F, Dowsett M, Schiff R, Brown M. 2017. Embryonic transcription factor SOX9 drives breast cancer endocrine resistance. Proc Natl Acad Sci. 114:E4482–E4491.

Kamakura S, Oishi K, Yoshimatsu T, Nakafuku M, Masuyama N, Gotoh Y. 2004. Hes binding to STAT3 mediates crosstalk between Notch and JAK–STAT signalling. Nat Cell Biol. 6:547–554.

Kang P, Lee HK, Glasgow SM, Finley M, Donti T, Gaber ZB, Graham BH, Foster AE, Novitch BG, Gronostajski RM, Deneen B. 2012. Sox9 and NFIA Coordinate a Transcriptional Regulatory Cascade during the Initiation of Gliogenesis. Neuron. 74:79–94.

Kanski R, van Strien ME, van Tijn P, Hol EM. 2014. A star is born: new insights into the mechanism of astrogenesis. Cell Mol Life Sci. 71:433–447.

Kao HY, Ordentlich P, Koyano-Nakagawa N, Tang Z, Downes M, Kintner CR, Evans RM, Kadesch T. 1998. A histone deacetylase corepressor complex regulates the Notch signal transduction pathway. Genes Dev. 12:2269–2277.

Li J, Chang HW, Lai E, Parker EJ, Vogt PK. 1995. The oncogene qin codes for a transcriptional repressor. Cancer Res. 55:5540–5544.

Magavi S, Friedmann D, Banks G, Stolfi A, Lois C. 2012. Coincident Generation of Pyramidal Neurons and Protoplasmic Astrocytes in Neocortical Columns. J Neurosci. 32:4762–4772.

Malatesta P, Appolloni I, Calzolari F. 2008. Radial glia and neural stem cells. Cell Tissue Res. 331:165–178.

Mallamaci A. 2013. Developmental control of cortico-cerebral astrogenesis. Int J Dev Biol. 57:689–706.

Manuel M, Martynoga B, Yu T, West JD, Mason JO, Price DJ. 2010. The transcription factor Foxg1 regulates the competence of telencephalic cells to adopt subpallial fates in mice. Development. 137:487–497.

Mariani J, Coppola G, Zhang P, Abyzov A, Provini L, Tomasini L, Amenduni M, Szekely A, Palejev D, Wilson M, Gerstein M, Grigorenko EL, Chawarska K, Pelphrey KA, Howe JR, Vaccarino FM. 2015. FOXG1-Dependent Dysregulation of GABA/Glutamate Neuron Differentiation in Autism Spectrum Disorders. Cell. 162:375–390.

Mathelier A, Zhao X, Zhang AW, Parcy F, Worsley-Hunt R, Arenillas DJ, Buchman S, Chen C, Chou A, Ienasescu H, Lim J, Shyr C, Tan G, Zhou M, Lenhard B, Sandelin A, Wasserman WW. 2014. JASPAR 2014: an extensively expanded and updated open-access database of transcription factor binding profiles. Nucleic Acids Res. 42:D142-147.

Miller FD, Gauthier AS. 2007. Timing is everything: making neurons versus glia in the developing cortex. Neuron. 54:357–369.

Miyoshi G, Fishell G. 2012. Dynamic FoxG1 Expression Coordinates the Integration of Multipolar Pyramidal Neuron Precursors into the Cortical Plate. Neuron. 74:1045–1058.

Morrow T, Song MR, Ghosh A. 2001. Sequential specification of neurons and glia by developmentally regulated extracellular factors. Dev Camb Engl. 128:3585–3594.

Muzio L, Mallamaci A. 2005. Foxg1 confines Cajal-Retzius neuronogenesis and hippocampal morphogenesis to the dorsomedial pallium. J Neurosci. 25:4435–4441.

Nagao M, Ogata T, Sawada Y, Gotoh Y. 2016. Zbtb20 promotes astrocytogenesis during neocortical development. Nat Commun. 7:11102.

Naka H, Nakamura S, Shimazaki T, Okano H. 2008. Requirement for COUP-TFI and II in the temporal specification of neural stem cells in CNS development. Nat Neurosci.

Nakashima K. 1999. Synergistic Signaling in Fetal Brain by STAT3-Smad1 Complex Bridged by p300. Science. 284:479–482.

Namihira M, Kohyama J, Semi K, Sanosaka T, Deneen B, Taga T, Nakashima K. 2009. Committed Neuronal Precursors Confer Astrocytic Potential on Residual Neural Precursor Cells. Dev Cell. 16:245–255.

Nielsen JV, Blom JB, Noraberg J, Jensen NA. 2010. Zbtb20-Induced CA1 Pyramidal Neuron Development and Area Enlargement in the Cerebral Midline Cortex of Mice. Cereb Cortex. 20:1904–1914.

Nielsen JV, Nielsen FH, Ismail R, Noraberg J, Jensen NA. 2007. Hippocampus-like corticoneurogenesis induced by two isoforms of the BTB-zinc finger gene Zbtb20 in mice. Dev Camb Engl. 134:1133–1140.

Ohtsuka T, Shimojo H, Matsunaga M, Watanabe N, Kometani K, Minato N, Kageyama R. 2011. Gene Expression Profiling of Neural Stem Cells and Identification of Regulators of Neural Differentiation During Cortical Development. STEM CELLS. 29:1817–1828.

Okamoto M, Miyata T, Konno D, Ueda HR, Kasukawa T, Hashimoto M, Matsuzaki F, Kawaguchi A. 2016. Cell-cycle-independent transitions in temporal identity of mammalian neural progenitor cells. Nat Commun. 7:11349.

Okano H, Temple S. 2009. Cell types to order: temporal specification of CNS stem cells. Curr Opin Neurobiol. 19:112–119.

Patriarchi T, Amabile S, Frullanti E, Landucci E, Lo Rizzo C, Ariani F, Costa M, Olimpico F, W Hell J, M Vaccarino F, Renieri A, Meloni I. 2016. Imbalance of excitatory/inhibitory synaptic protein expression in iPSC-derived neurons from FOXG1(+/-) patients and in foxg1(+/-) mice. Eur J Hum Genet EJHG. 24:871–880.

Pluchino S, Gritti A, Blezer E, Amadio S, Brambilla E, Borsellino G, Cossetti C, Del Carro U, Comi G, 't Hart B, Vescovi A, Martino G. 2009. Human neural stem cells ameliorate autoimmune encephalomyelitis in non-human primates. Ann Neurol. 66:343–354.

Pontrelli G, Cappelletti S, Claps D, Sirleto P, Ciocca L, Petrocchi S, Terracciano A, Serino D, Fusco L, Vigevano F, Specchio N. 2014. Epilepsy in Patients With Duplications of Chromosome 14 Harboring FOXG1. Pediatr Neurol. 50:530–535.

Qian X, Shen Q, Goderie SK, He W, Capela A, Davis AA, Temple S. 2000. Timing of CNS cell generation: a programmed sequence of neuron and glial cell production from isolated murine cortical stem cells. Neuron. 28:69–80.

Raponi E, Agenes F, Delphin C, Assard N, Baudier J, Legraverend C, Deloulme J-C. 2007. S100B expression defines a state in which GFAP-expressing cells lose their neural stem cell potential and acquire a more mature developmental stage. Glia. 55:165–177.

Rodriguez C, Huang LJ-S, Son JK, McKee A, Xiao Z, Lodish HF. 2001. Functional Cloning of the Proto-oncogene Brain Factor-1 (BF-1) As a Smad-binding Antagonist of Transforming Growth Factor-β Signaling. J Biol Chem. 276:30224–30230.

Sardi SP, Murtie J, Koirala S, Patten BA, Corfas G. 2006. Presenilin-Dependent ErbB4 Nuclear Signaling Regulates the Timing of Astrogenesis in the Developing Brain. Cell. 127:185–197.

Schlessinger J, Lemmon MA. 2006. Nuclear Signaling by Receptor Tyrosine Kinases: The First Robin of Spring. Cell. 127:45–48.

Sloan SA, Barres BA. 2014. Mechanisms of astrocyte development and their contributions to neurodevelopmental disorders. Curr Opin Neurobiol. 27:75–81.

Sun Y, Nadal-Vicens M, Misono S, Lin MZ, Zubiaga A, Hua X, Fan G, Greenberg ME. 2001. Neurogenin promotes neurogenesis and inhibits glial differentiation by independent mechanisms. Cell. 104:365–376.

Takouda J, Katada S, Nakashima K. 2017. Emerging mechanisms underlying astrogenesis in the developing mammalian brain. Proc Jpn Acad Ser B. 93:386–398.

Toma K, Kumamoto T, Hanashima C. 2014. The timing of upper-layer neurogenesis is conferred by sequential derepression and negative feedback from deep-layer neurons. J Neurosci Off J Soc Neurosci. 34:13259–13276.

Tonchev AB, Tuoc TC, Rosenthal EH, Studer M, Stoykova A. 2016. Zbtb20 modulates the sequential generation of neuronal layers in developing cortex. Mol Brain. 9.

Tsai H-H, Li H, Fuentealba LC, Molofsky AV, Taveira-Marques R, Zhuang H, Tenney A, Murnen AT, Fancy SPJ, Merkle F, Kessaris N, Alvarez-Buylla A, Richardson WD, Rowitch DH. 2012. Regional Astrocyte Allocation Regulates CNS Synaptogenesis and Repair. Science. 337:358–362.

Vainchenker W. 2005. A Unique Activating Mutation in JAK2 (V617F) Is at the Origin of Polycythemia Vera and Allows a New Classification of Myeloproliferative Diseases. Hematology. 2005:195–200.

Yao J, Lai E, Stifani S. 2001. The winged-helix protein brain factor 1 interacts with groucho and hes proteins to repress transcription. Mol Cell Biol. 21:1962–1972.

LEGEND TO FIGURES

Figure 1. *Foxg1* antagonizes astrogenic progression of murine cortico-cerebral stem cells. (A-G) *In vivo* analysis. (A-C) Experimental strategies, (D) lentiviral vectors employed, and (E-G) results. (E, left) (ctr)-normalized frequencies of Nestin$^+$ derivatives of E12.5 neocortical (ncx) precursors, acutely infected as in (A, analysis 1) [absolute frequency of Nestin$^+$ cells in (ctr) samples, 10.38±0.39%]. Analysis performed on cells acutely attached on poly-L-lysin-coated coverslips. (E, right) Absolute frequencies of S100β$^+$ astrocytes, evaluated within the parietal cortex of P4 pups among derivatives of cells engineered as in (A, analysis 2), and co-transplanted as a 1:1 mix into the cortical parietal parenchyma of isochronic P0 pups [average parameter value in (ctr) samples, 30.38±2.24%]. (F, left) (ctr)-normalized-frequencies of Nestin$^+$ derivatives of E12.5 neocortical precursors, acutely infected as in (B, analysis 1) [absolute frequency of Nestin$^+$ cells in (ctr) samples, 22.45±1.21%]. Analysis performed on cells acutely attached on poly-L-lysin-coated coverslips. (F, right) Absolute frequencies of S100β$^+$ astrocytes, evaluated within the parietal cortex of P4 pups among derivatives of cells engineered as in (B, analysis 2), and co-transplanted as a 1:1 mix into the cortical parietal parenchyma of heterochronic P0 pups [average parameter value in (ctr) samples, 25.04±2.85%]. (G) Absolute frequencies of S100β$^+$ astrocytes, evaluated within the parietal cortex of P4 pups among derivatives of cells engineered as in (C), and co-transplanted as a 1:1 mix into the cortical parietal parenchyma of isochronic E14.5 wild-type embryos [average parameter value in (ctr) samples, 36.27±4.77%]. **(H-K)** *In vitro* analysis: neural cell frequencies, long protocol. (H,J) Experimental strategy and lentiviral vectors employed for its implementation, and (I,K) results. (I) Results of GOF analysis referred to in (H). Analysis 1: ctr-normalized frequencies of Sox2$^+$-mCherry$^-$ cells at DIV4 [absolute (ctr) frequency, 15.05±0.79%]. Cells acutely attached on poly-L-lysin-coated coverslips. Analysis 2 results: ctr-normalized frequencies of S100β$^+$, Gfap$^+$ and Tubb3$^+$ cells at DIV11 [absolute (ctr) frequencies, 14.95±1.27%, 21.67±1.03% and 16.85±3.00%, respectively]. (K) Results of LOF analysis referred to in (J). Analysis 1: Ctr-normalized frequencies of Sox2$^+$-mCherry$^-$ cells at DIV4 [absolute (ctr) frequency, 14.36±0.10%]. Cells acutely attached on poly-L-lysin-coated coverslips. Analysis 2: ctr-normalized frequencies of S100β$^+$ cells at DIV11 [absolute (ctr) frequency, 25.36±1.70%]. **(L,M)** *In vitro* analysis: neural cell frequencies, short protocol. (L) Experimental strategy, lentiviral vectors employed, and (M) results. Here shown are (ctr)-normalized frequencies of Gfap$^+$ cells *among Egfp-expressing derivatives* of engineered neocortical precursors [absolute (ctr) parameter value,19.06±0.85%]. **(N-P)** *In vitro* analysis: clonal assays. (N) Experimental strategy, lentiviral vectors employed, and (O,P) results. Here shown are absolute frequencies of Tubβ3$^+$Gfap$^-$ (neuron-only), Tubβ3$^-$Gfap$^+$ (astrocyte-only), Tubβ3$^+$Gfap$^+$ (neuron-astrocyte-mixed) clones, as evaluated among total clones originating from E11.5 neocortical precursors, infected and processed as in (N). **(Q,R)** *In vitro* analysis: cell-autonomous vs non-cell-autonomous mechanisms. (Q) Experimental strategy, lentiviral vectors employed, and (R) results. Here, shown are (ctr)-normalized

$Gfap^+mCherry^+/mCherry^+$ and $Gfap^+mCherry^-/mCherry^-$ cell number ratios, as well as (ctr)-normalized $mCherry^+$ cell frequencies, as evaluated in DIV11 cultures originating from of E12.5 neocortical (ncx) precursors, acutely infected and processed as in (Q). [absolute (ctr) parameter values, 56.50±1.70%, 41.57±1.78%, and 16.12±1.49%, respectively]. Error bar = s.e.m. *n* is the number of biological replicates (i.e. independently transduced cell samples, or - case (E, right), (F, right) and (G) - co-transplanted brains). *p*-value calculated by t-test (one-tail, unpaired, or - case (E, right), (F, right) and (G) - one-tail, paired).

Figure 2. *Foxg1* downregulates key effectors directing NSCs to astrogenic fates. (A-F) Impact of *Foxg1* manipulation on *Couptf1, Zbtb20*, *Sox9* and *Nfia* mRNA levels in late embryonic cortico-cerebral precursors. (A,B) Experimental protocols, (C) lentiviral vectors employed, and (D-F) results [(D) referring to (A), (E,F) to (B)]. Data double-normalized, against endogenous *Gapdh*-mRNA and (ctr) values**. (G-I)** Functional relevance of *Zbtb20* and *Nfia* misregulation to *Foxg1* antiastrogenic activity. This was tested by antagonizing *Foxg1*-driven expression changes of these effectors and interrogating the engineered cultures by clonal analysis, similar to Fig. 1N,O. (G) Experimental protocol, (C) lentiviral vectors employed, and (H,I) results. **(J,K)** Chromatin ImmunoPrecipitation-PCR (qChIP-PCR) quantification of Foxg1-enrichment at putative Foxg1 binding sites within *Couptf1*, *Zbtb20*, *Sox9* and *Nfia* loci (named as in Fig. S2A-D): (J) experimental protocol and (K) results. Data normalized against input chromatin. Error bar = s.e.m. *n* is the number of biological replicates (i.e. independently transduced cell samples). *p*-value calculated by t-test (one-tail, unpaired).

Figure 3. Foxg1 represses astroglial-lineage active genes. (A,B) Regulation of astroglial *Gfap*, *S100β* and *Aqp4* genes by *Foxg1*: (A) experimental strategy, lentiviral vectors employed, and (B) results. Data double-normalized, against endogenous *Gapdh*-mRNA and (ctr) values. **(C,D)** Assaying direct regulation mechanisms: Chromatin ImmunoPrecipitation-PCR (qChIP-PCR) quantification of Foxg1-enrichment at putative Foxg1 binding sites within *Gfap*, *S100b* and *Aqp4* loci (named as in Fig. S2E-G): (C) experimental strategy, lentiviral vectors employed, and (D) results. Data normalized, against input chromatin. **(E-J)** Assaying indirect regulation mechanisms**.** (E,G) Modulation of nuclear pStat3, pSmad1,5,8, $ErbB4^{ICD}$, NCoR1, $Notch1^{ICD}$ protein levels in $Nestin^+$, E12.5+DIV7 neural stem cells (NSCs), overexpressing *Foxg1,* evaluation by quantitative immunofluorescence. (E) Experimental protocol, lentiviral vectors employed, and (G) results. Data normalized against (ctr). (F,H) Functional relevance of pStat3, pSmad1,5,8, $ErbB4I^{CD}$, NCoR1 and $Notch1^{ICD}$ misregulation to *Foxg1* antiastrogenic activity, assessed by counteracting *Foxg1*-driven changes of these effectors and evaluating the resulting $S100\beta^+$ cell frequency. Constitutively active Stat3 and Smad1 (caStat3 and caSmad1) were overexpressed one by one or combined; functional relevance of $ErbB4^{ICD}$ and NCoR1 was investigated by dampening their essential Tab2 cofactor. (F) Experimental protocol, lentiviral vectors employed, and (H) results. Data normalized against (ctr); absolute frequencies of $S100\beta^+$ cells: 11.84±2.30% (ctr_{pStat3}),

8.58±0.43% ($ctr_{pSmad1,5,8}$), 8.87±0.62% ($ctr_{pStat3\text{-}pSmad1,5,8}$), 21.36±5.27% ($ctr_{Tab2}$); absolute frequencies of $Gfap^+$ cells: 37.59±3.14% ($ctr_{Notch1\text{-}ICD}$). Data normalized against (ctr). Error bar = s.e.m. *n* is the number of biological replicates. These are: (B,D,H) independently transduced neural cultures; (G) single cells, randomly and evenly picked from 4,4 independently transduced neural cultures. *p*-values calculated by t-test (one-tail, unpaired).

Figure 4. Molecular details of *Foxg1* impact on different astrogenic pathways. (A-C) Consequences of *Foxg1* manipulation on mRNA levels of *IL6Ra*, *Gp130*, *Jak2*, *Stat3*, *Bmp4*, *BmpRII*, *NCoR1*. (A) Experimental protocol and lentiviral vectors employed, (B-C) results. Data double-normalized, against endogenous *Gapdh*-mRNA and (ctr) values. **(D,E)** Functional relevance of *Jak2* misregulation to *Foxg1* antiastrogenic activity. This was assessed by counteracting *Foxg1*-driven change of *Jak2*-mRNA and evaluating the resulting $S100\beta^+$ cell frequency: (D) experimental protocol and lentiviral vectors employed, (E) results. Data normalized against (ctr); absolute frequency of $S100\beta^+$ cells in (ctr) samples: 28.70±0.81%. (**F,G**) Foxg1 impact on trans-activating abilities of BMP/Jak-Stat pathways effectors. This was assessed by expressing caStat3 and caSmad1 in E12.5 neocortical precursor cultures and evaluating their ability to transactivate a lentivector-delivered, randomly integrating fluorescent reporter gene, associated to Bmp responsive elements (BMP-RE), upon *Foxg1* overexpression. (F) Experimental protocol, lentiviral vectors employed, and (G) (ctr)-normalized results. Analysis by cytofluorometry. Absolute (ctr) frequency of $ZsGreen^+$ cells: 78.50±5.33%. Error bar = s.e.m. *n* is the number of biological replicates. *p*-values calculated by t-test (one-tail, unpaired).

Figure 5. Neocortical stem cell Foxg1 levels decrease prior to the neocortical astrogenic wave. (A,C) *Foxg1*-mRNA levels in *in vitro* aging neural stem cells, labelled by lentiviral tracers, identified as pNes-$Egfp^+$/pTα1-$mCherry^-$ and purified by FACsorting. In (A) experimental protocol, in (C) results. *Ngn1* and *Zbtb20* are shown as controls. Data double-normalized, against endogenous *Gapdh*-mRNA and "E11.5+DIV2" values. **(B,D,E)** Foxg1-protein levels in *in vitro* aging neural stem cells, recognized as $Nestin^+$ cells and scored by quantitative immunofluorescence. In (B) experimental protocol, in (D) results and in (E) example pictures. Data normalized against E12.5 average value. Empty arrowheads in (E) point to $Nestin^+$ elements. **(F)** *In vivo* distribution of Foxg1 protein in neocortical periventricular layers of E12.5 and E16.5 embryos. **(G,H)** Foxg1-protein levels in acutely dissociated, $Nestin^+$ neural stem cells taken from E12.5 and E16.5 neocortices, scored by quantitative immunofluorescence. In (G) results, in (H) localization of sampled cells, in (I) primary data examples. Empty arrowheads in (I) point to $Nestin^+$ elements. Error bar = s.e.m. *n* is the number of biological replicates. These are: (C) independently transduced neural cultures, or (D,H) single cells, randomly and evenly picked from 4,4 independently transduced neural cultures (D) and 4,4 acutely dissociated neocortices (H). *p*-values calculated by t-test (one-tail, unpaired).

Figure 6. Foxg1 inhibits progression of human pallial precursors towards astrogenesis. (A-C) Impact of *FOXG1* modulation on astrogenic outputs of engineered human neocortical precursors: temporal articulation of the histogenetic assays, lentiviral vectors employed, and results. The tests were run on late human neocortical precursors, derived from PCW10 abortions and pre-expanded in vitro over 150 (A,B) or 120 (C) days. Astrocytic outputs were evaluated upon (A) constitutive (pPgk1-rtTA^{M2}-driven) or (B) NSC-restricted (pNestin-rtTA^{M2}-driven) *Foxg1*-GOF manipulations, as well as upon (C) constitutive *FOXG1* knock-down via a U6 promoter-driven, *αFoxg1*-shRNA transgene (*FOXG1*-LOF samples). Shown are control-normalized frequencies of S100β^{+} (A) and GFAP^{+} (B,C) cells, and pNesEgfp^{+}GFAP^{-} NSCs (C), as well as control-normalized GFAP^{+}/pNesEgfp^{+}GFAP^{-} cell ratios (C). Absolute control frequencies of S100β^{+} cells (A), GFAP^{+} cells (B), pNesEgfp^{-}GFAP^{+} cells (C) and pNesEgfp^{+}GFAP$^{\pm}$ NSCs (C), 24.70±4.00%, 12.62±0.46%, 23.38±1.45% and 44.16±2.54%, respectively. **(D)** Modulation of putative genes and pathways mediating the impact of *FOXG1* downregulation on astrogenesis: protocols, lentiviruses employed and results. Shown are control/*GADPH*-double-normalized, *FOXG1*, *COUPTF1*, *ZBTB20*, *SOX9* and *NFIA* mRNA levels, as well as control/*mCherry*-double-normalized, *Egfp* (pStat1,3-RE-Egfp) and *ZsGreen* (BMP-RE-ZsGreen) mRNA levels. Error bar = s.e.m. *n* is the number of biological replicates, i.e. independently transduced neural cultures. *p*-values calculated by t-test (one-tail, unpaired).

Figure 7. *Foxg1* control of astrogenesis: a graphical synopsis. (A) *Foxg1* impact on early effectors endowing NSCs with astrogenic competence. **(B)** Foxg1 modulation of genes implementing the astroglial differentiation program and their cardinal regulators.

Fig. 1

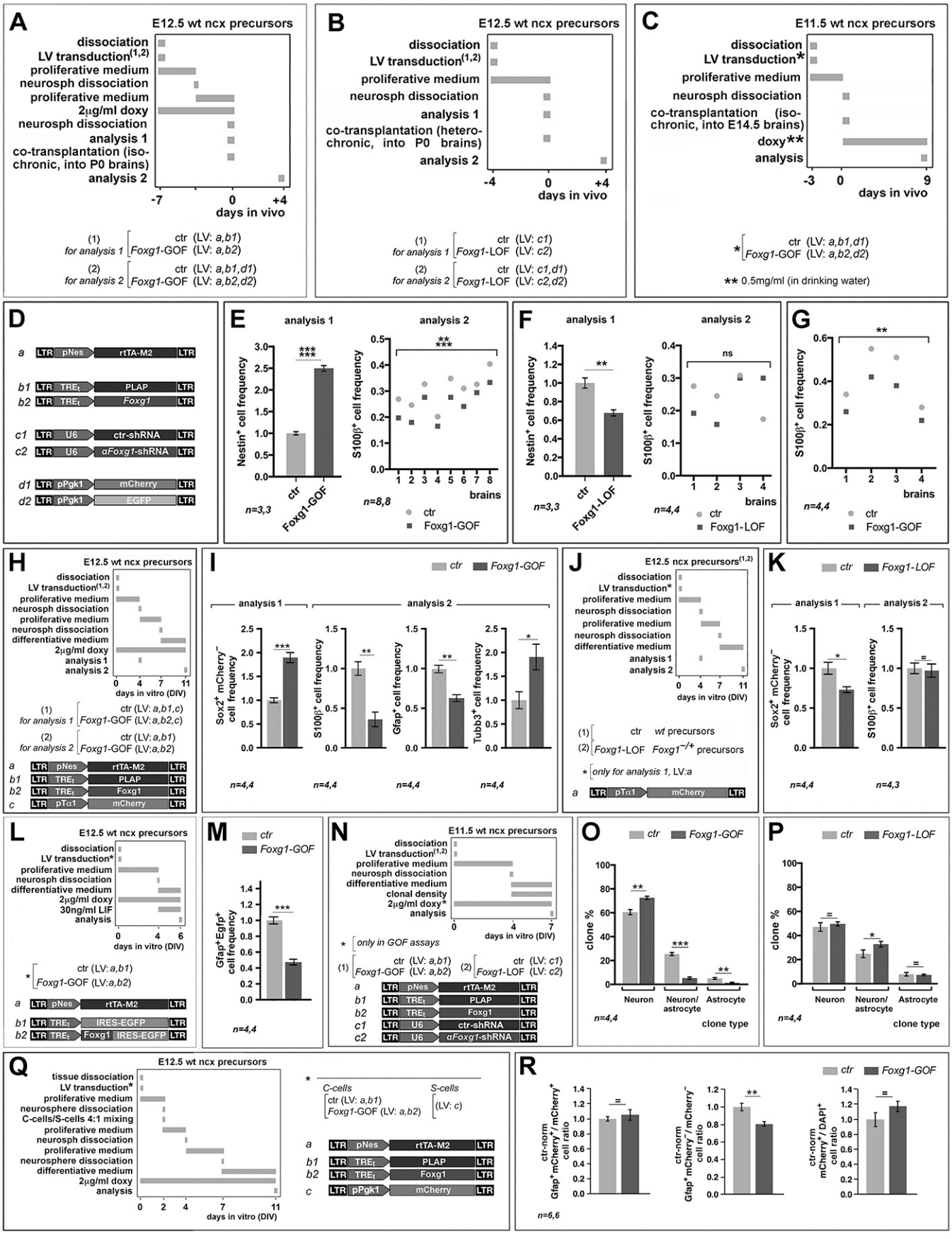
A
E12.5 wt ncx precursors
dissociation
LV transduction(1,2)
proliferative medium
neurosph dissociation
proliferative medium
2µg/ml doxy
neurosph dissociation
analysis 1
co-transplantation (iso-chronic, into P0 brains)
analysis 2
-7
0
+4
days in vivo
(1) for analysis 1: ctr (LV: a,b1); Foxg1-GOF (LV: a,b2)
(2) for analysis 2: ctr (LV: a,b1,d1); Foxg1-GOF (LV: a,b2,d2)
B
E12.5 wt ncx precursors
dissociation
LV transduction(1,2)
proliferative medium
neurosph dissociation
analysis 1
co-transplantation (hetero-chronic, into P0 brains)
analysis 2
-4
0
+4
days in vivo
(1) for analysis 1: ctr (LV: c1); Foxg1-LOF (LV: c2)
(2) for analysis 2: ctr (LV: c1,d1); Foxg1-LOF (LV: c2,d2)
C
E11.5 wt ncx precursors
dissociation
LV transduction*
proliferative medium
neurosph dissociation
co-transplantation (iso-chronic, into E14.5 brains)
doxy**
analysis
-3
0
9
days in vivo
*: ctr (LV: a,b1,d1); Foxg1-GOF (LV: a,b2,d2)
** 0.5mg/ml (in drinking water)
D
a LTR pNes rtTA-M2 LTR
b1 LTR TREt PLAP LTR
b2 LTR TREt Foxg1 LTR
c1 LTR U6 ctr-shRNA LTR
c2 LTR U6 αFoxg1-shRNA LTR
d1 LTR pPgk1 mCherry LTR
d2 LTR pPgk1 EGFP LTR
E
analysis 1
analysis 2
Nestin+ cell frequency
S100β+ cell frequency
***
**
ctr
Foxg1-GOF
n=3,3
n=8,8
brains
F
analysis 1
analysis 2
Nestin+ cell frequency
S100β+ cell frequency
**
ns
ctr
Foxg1-LOF
n=3,3
n=4,4
brains
G
S100β+ cell frequency
**
n=4,4
brains
ctr
Foxg1-GOF
H
E12.5 wt ncx precursors
dissociation
LV transduction(1,2)
proliferative medium
neurosph dissociation
proliferative medium
neurosph dissociation
differentiative medium
2µg/ml doxy
analysis 1
analysis 2
days in vitro (DIV)
(1) for analysis 1: ctr (LV: a,b1,c); Foxg1-GOF (LV:a,b2,c)
(2) for analysis 2: ctr (LV:a,b1); Foxg1-GOF (LV:a,b2)
a LTR pNes rtTA-M2 LTR
b1 LTR TREt PLAP LTR
b2 LTR TREt Foxg1 LTR
c LTR pTα1 mCherry LTR
I
ctr
Foxg1-GOF
analysis 1
analysis 2
Sox2+ mCherry− cell frequency
S100β+ cell frequency
Gfap+ cell frequency
Tubb3+ cell frequency
n=4,4
J
E12.5 ncx precursors(1,2)
dissociation
LV transduction*
proliferative medium
neurosph dissociation
proliferative medium
neurosph dissociation
differentiative medium
analysis 1
analysis 2
days in vitro (DIV)
(1) ctr wt precursors
(2) Foxg1-LOF Foxg1−/+ precursors
* only for analysis 1, LV:a
a LTR pTα1 mCherry LTR
K
ctr
Foxg1-LOF
analysis 1
analysis 2
Sox2+ mCherry− cell frequency
S100β+ cell frequency
n=4,4
n=4,3
L
E12.5 wt ncx precursors
dissociation
LV transduction*
proliferative medium
neurosph dissociation
differentiative medium
2µg/ml doxy
30ng/ml LIF
analysis
days in vitro (DIV)
*: ctr (LV:a,b1); Foxg1-GOF (LV:a,b2)
a LTR pNes rtTA-M2 LTR
b1 LTR TREt IRES-EGFP LTR
b2 LTR TREt Foxg1 IRES-EGFP LTR
M
ctr
Foxg1-GOF
Gfap+Egfp+ cell frequency
***
n=4,4
N
E11.5 wt ncx precursors
dissociation
LV transduction(1,2)
proliferative medium
neurosph dissociation
differentiative medium
clonal density
2µg/ml doxy*
analysis
days in vitro (DIV)
* only in GOF assays
(1) ctr (LV: a,b1); Foxg1-GOF (LV: a,b2)
(2) ctr (LV: c1); Foxg1-LOF (LV: c2)
a LTR pNes rtTA-M2 LTR
b1 LTR TREt PLAP LTR
b2 LTR TREt Foxg1 LTR
c1 LTR U6 ctr-shRNA LTR
c2 LTR U6 αFoxg1-shRNA LTR
O
ctr
Foxg1-GOF
clone %
Neuron
Neuron/ astrocyte
Astrocyte
clone type
n=4,4
P
ctr
Foxg1-LOF
clone %
Neuron
Neuron/ astrocyte
Astrocyte
clone type
n=4,4
Q
E12.5 wt ncx precursors
tissue dissociation
LV transduction*
proliferative medium
neurosphere dissociation
C-cells/S-cells 4:1 mixing
proliferative medium
neurosph dissociation
proliferative medium
neurosphere dissociation
differentiative medium
2µg/ml doxy
analysis
days in vitro (DIV)
*: C-cells: ctr (LV: a,b1); Foxg1-GOF (LV: a,b2); S-cells: (LV: c)
a LTR pNes rtTA-M2 LTR
b1 LTR TREt PLAP LTR
b2 LTR TREt Foxg1 LTR
c LTR pPgk1 mCherry LTR
R
ctr
Foxg1-GOF
ctr-norm Gfap+mCherry+/mCherry+ cell ratio
ctr-norm Gfap+mCherry+/mCherry− cell ratio
ctr-norm mCherry+/DAPI+ cell ratio
n=6,6

Fig. 2

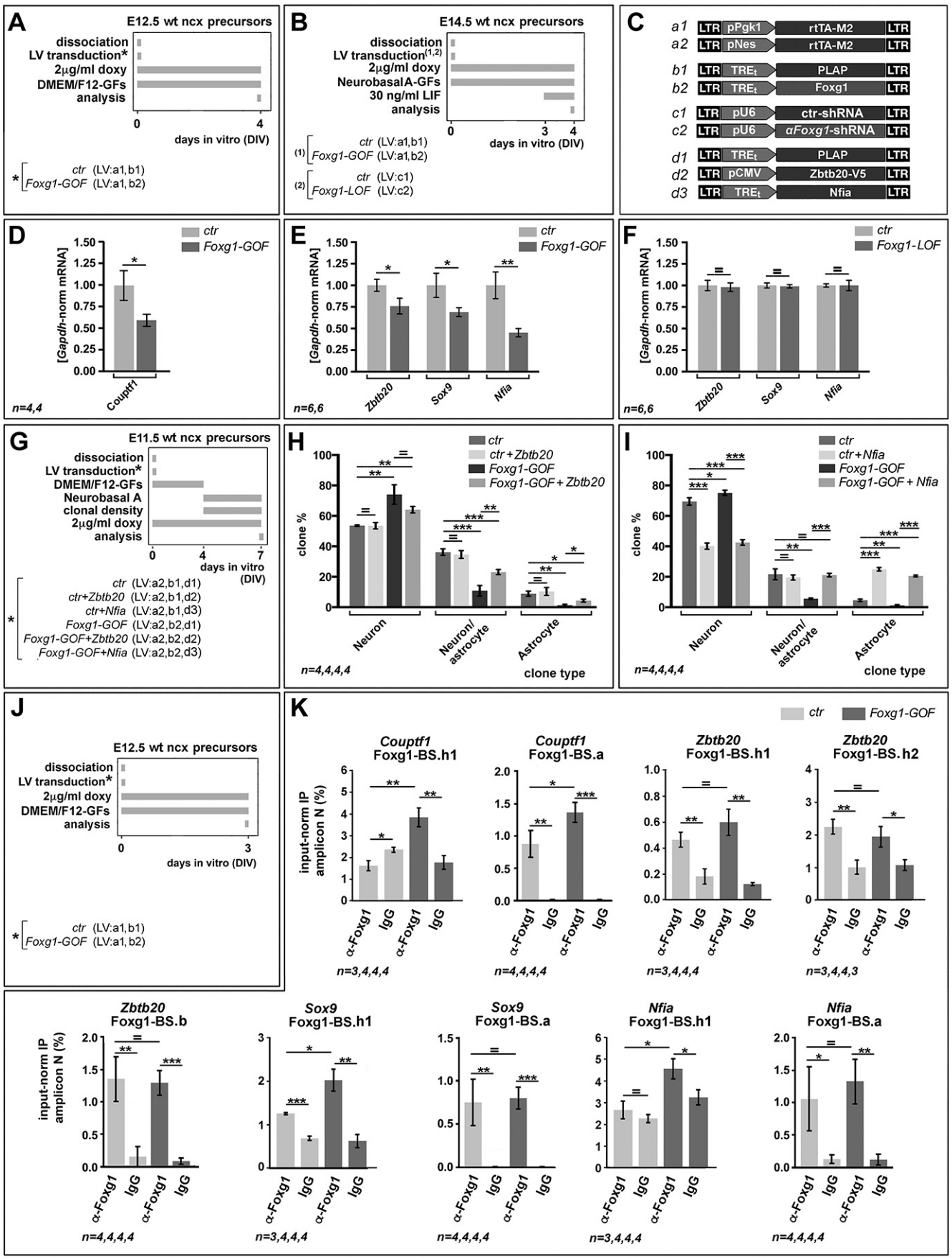
A
E12.5 wt ncx precursors
dissociation
LV transduction*
2µg/ml doxy
DMEM/F12-GFs
analysis
0
4
days in vitro (DIV)
* ctr (LV:a1,b1)
Foxg1-GOF (LV:a1,b2)
B
E14.5 wt ncx precursors
dissociation
LV transduction(1,2)
2µg/ml doxy
NeurobasalA-GFs
30 ng/ml LIF
analysis
0
3
4
days in vitro (DIV)
(1) ctr (LV:a1,b1)
Foxg1-GOF (LV:a1,b2)
(2) ctr (LV:c1)
Foxg1-LOF (LV:c2)
C
a1 LTR pPgk1 rtTA-M2 LTR
a2 LTR pNes rtTA-M2 LTR
b1 LTR TRE$_t$ PLAP LTR
b2 LTR TRE$_t$ Foxg1 LTR
c1 LTR pU6 ctr-shRNA LTR
c2 LTR pU6 αFoxg1-shRNA LTR
d1 LTR TRE$_t$ PLAP LTR
d2 LTR pCMV Zbtb20-V5 LTR
d3 LTR TRE$_t$ Nfia LTR
D
ctr
Foxg1-GOF
[Gapdh-norm mRNA]
Couptf1
n=4,4
E
ctr
Foxg1-GOF
[Gapdh-norm mRNA]
Zbtb20
Sox9
Nfia
n=6,6
F
ctr
Foxg1-LOF
[Gapdh-norm mRNA]
Zbtb20
Sox9
Nfia
n=6,6
G
E11.5 wt ncx precursors
dissociation
LV transduction*
DMEM/F12-GFs
Neurobasal A
clonal density
2µg/ml doxy
analysis
0
4
7
days in vitro (DIV)
* ctr (LV:a2,b1,d1)
ctr+Zbtb20 (LV:a2,b1,d2)
ctr+Nfia (LV:a2,b1,d3)
Foxg1-GOF (LV:a2,b2,d1)
Foxg1-GOF+Zbtb20 (LV:a2,b2,d2)
Foxg1-GOF+Nfia (LV:a2,b2,d3)
H
ctr
ctr+Zbtb20
Foxg1-GOF
Foxg1-GOF+Zbtb20
clone %
Neuron
Neuron/ astrocyte
Astrocyte
clone type
n=4,4,4,4
I
ctr
ctr+Nfia
Foxg1-GOF
Foxg1-GOF+Nfia
clone %
Neuron
Neuron/ astrocyte
Astrocyte
clone type
n=4,4,4,4
J
E12.5 wt ncx precursors
dissociation
LV transduction*
2µg/ml doxy
DMEM/F12-GFs
analysis
0
3
days in vitro (DIV)
* ctr (LV:a1,b1)
Foxg1-GOF (LV:a1,b2)
K
ctr
Foxg1-GOF
Couptf1 Foxg1-BS.h1
Couptf1 Foxg1-BS.a
Zbtb20 Foxg1-BS.h1
Zbtb20 Foxg1-BS.h2
input-norm IP amplicon N (%)
α-Foxg1
IgG
n=3,4,4,4
n=4,4,4,4
n=3,4,4,4
n=3,4,4,3
Zbtb20 Foxg1-BS.b
Sox9 Foxg1-BS.h1
Sox9 Foxg1-BS.a
Nfia Foxg1-BS.h1
Nfia Foxg1-BS.a
n=4,4,4,4
n=3,4,4,4
n=4,4,4,4
n=3,4,4,4
n=4,4,4,4

Fig. 3

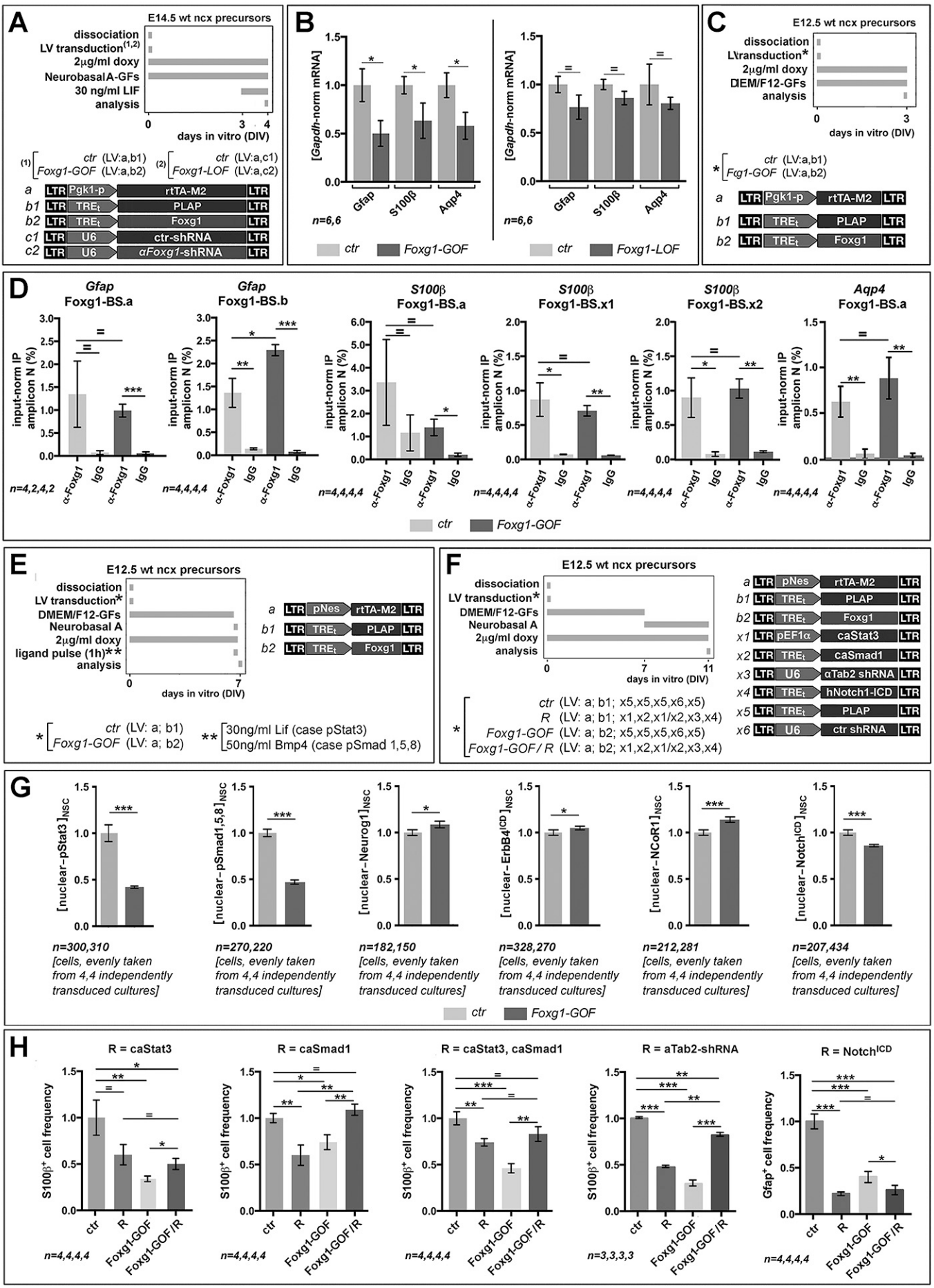
A
E14.5 wt ncx precursors
dissociation
LV transduction(1,2)
2μg/ml doxy
NeurobasalA-GFs
30 ng/ml LIF
analysis
days in vitro (DIV)
(1) ctr (LV:a,b1) Foxg1-GOF (LV:a,b2)
(2) ctr (LV:a,c1) Foxg1-LOF (LV:a,c2)
a LTR Pgk1-p rtTA-M2 LTR
b1 LTR TREt PLAP LTR
b2 LTR TREt Foxg1 LTR
c1 LTR U6 ctr-shRNA LTR
c2 LTR U6 αFoxg1-shRNA LTR
B
[Gapdh-norm mRNA]
Gfap
S100β
Aqp4
n=6,6
ctr
Foxg1-GOF
Foxg1-LOF
C
E12.5 wt ncx precursors
dissociation
LVtransduction*
2μg/ml doxy
DMEM/F12-GFs
analysis
days in vitro (DIV)
* ctr (LV:a,b1) Fcg1-GOF (LV:a,b2)
a LTR Pgk1-p rtTA-M2 LTR
b1 LTR TREt PLAP LTR
b2 LTR TREt Foxg1 LTR
D
Gfap Foxg1-BS.a
Gfap Foxg1-BS.b
S100β Foxg1-BS.a
S100β Foxg1-BS.x1
S100β Foxg1-BS.x2
Aqp4 Foxg1-BS.a
input-norm IP amplicon N (%)
α-Foxg1
IgG
n=4,2,4,2
n=4,4,4,4
ctr
Foxg1-GOF
E
E12.5 wt ncx precursors
dissociation
LV transduction*
DMEM/F12-GFs
Neurobasal A
2μg/ml doxy
ligand pulse (1h)**
analysis
days in vitro (DIV)
a LTR pNes rtTA-M2 LTR
b1 LTR TREt PLAP LTR
b2 LTR TREt Foxg1 LTR
* ctr (LV: a; b1) Foxg1-GOF (LV: a; b2)
** 30ng/ml Lif (case pStat3) 50ng/ml Bmp4 (case pSmad 1,5,8)
F
E12.5 wt ncx precursors
dissociation
LV transduction*
DMEM/F12-GFs
Neurobasal A
2μg/ml doxy
analysis
days in vitro (DIV)
a LTR pNes rtTA-M2 LTR
b1 LTR TREt PLAP LTR
b2 LTR TREt Foxg1 LTR
x1 LTR pEF1α caStat3 LTR
x2 LTR TREt caSmad1 LTR
x3 LTR U6 αTab2 shRNA LTR
x4 LTR TREt hNotch1-ICD LTR
x5 LTR TREt PLAP LTR
x6 LTR U6 ctr shRNA LTR
* ctr (LV: a; b1; x5,x5,x5,x6,x5)
R (LV: a; b1; x1,x2,x1/x2,x3,x4)
Foxg1-GOF (LV: a; b2; x5,x5,x5,x6,x5)
Foxg1-GOF / R (LV: a; b2; x1,x2,x1/x2,x3,x4)
G
[nuclear-pStat3]NSC
[nuclear-pSmad1,5,8]NSC
[nuclear-Neurog1]NSC
[nuclear-ErbB4ICD]NSC
[nuclear-NCoR1]NSC
[nuclear-NotchICD]NSC
n=300,310 [cells, evenly taken from 4,4 independently transduced cultures]
n=270,220 [cells, evenly taken from 4,4 independently transduced cultures]
n=182,150 [cells, evenly taken from 4,4 independently transduced cultures]
n=328,270 [cells, evenly taken from 4,4 independently transduced cultures]
n=212,281 [cells, evenly taken from 4,4 independently transduced cultures]
n=207,434 [cells, evenly taken from 4,4 independently transduced cultures]
ctr
Foxg1-GOF
H
R = caStat3
R = caSmad1
R = caStat3, caSmad1
R = aTab2-shRNA
R = NotchICD
S100β+ cell frequency
Gfap+ cell frequency
ctr
R
Foxg1-GOF
Foxg1-GOF/R
n=4,4,4,4
n=3,3,3,3

Fig. 4

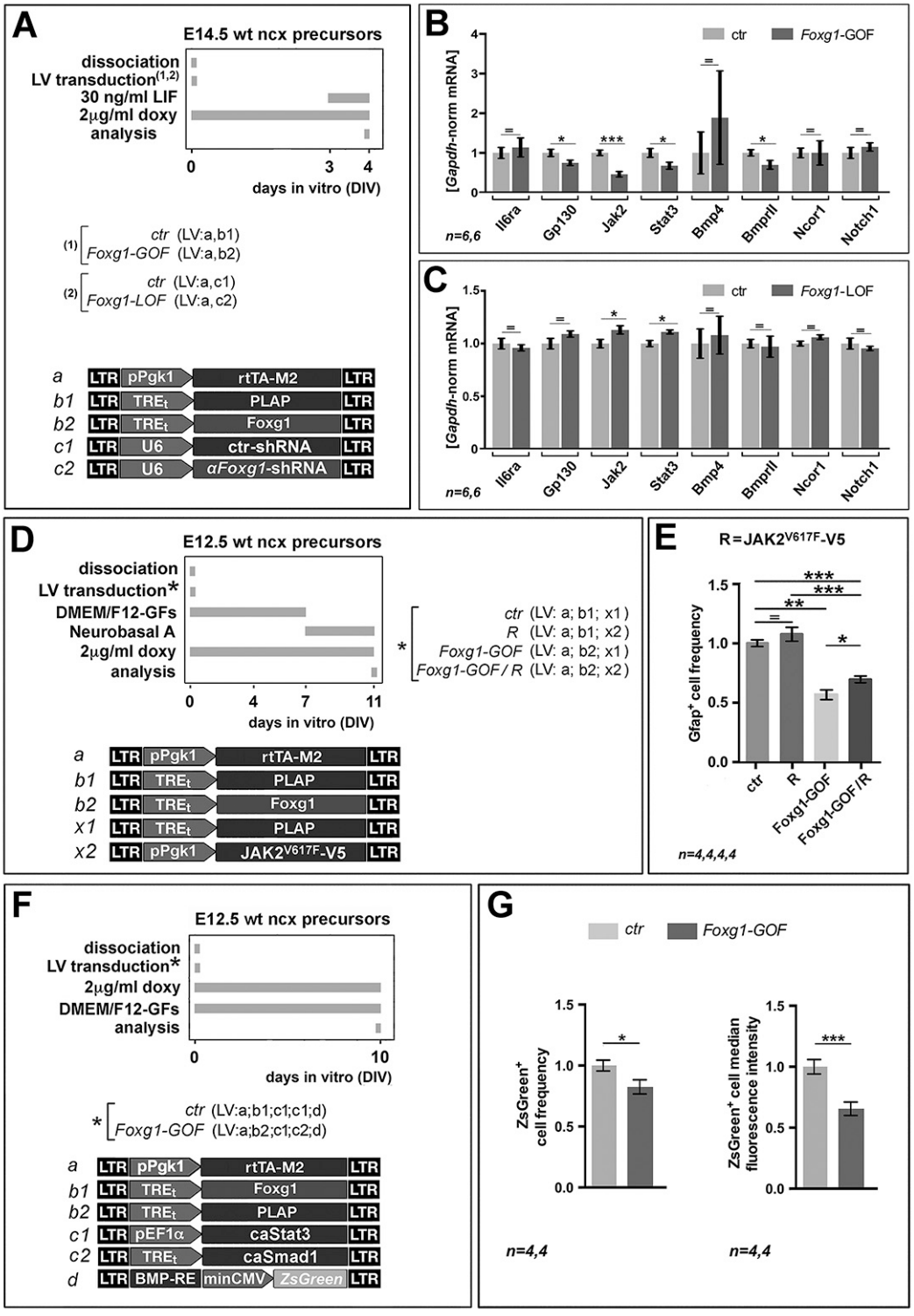
A
E14.5 wt ncx precursors
dissociation
LV transduction(1,2)
30 ng/ml LIF
2μg/ml doxy
analysis
0
3
4
days in vitro (DIV)
(1) ctr (LV:a,b1)
Foxg1-GOF (LV:a,b2)
(2) ctr (LV:a,c1)
Foxg1-LOF (LV:a,c2)
a LTR pPgk1 rtTA-M2 LTR
b1 LTR TREt PLAP LTR
b2 LTR TREt Foxg1 LTR
c1 LTR U6 ctr-shRNA LTR
c2 LTR U6 αFoxg1-shRNA LTR
B
ctr
Foxg1-GOF
[Gapdh-norm mRNA]
n=6,6
Il6ra
Gp130
Jak2
Stat3
Bmp4
BmprII
Ncor1
Notch1
C
ctr
Foxg1-LOF
[Gapdh-norm mRNA]
n=6,6
Il6ra
Gp130
Jak2
Stat3
Bmp4
BmprII
Ncor1
Notch1
D
E12.5 wt ncx precursors
dissociation
LV transduction*
DMEM/F12-GFs
Neurobasal A
2μg/ml doxy
analysis
0
4
7
11
days in vitro (DIV)
* ctr (LV: a; b1; x1)
R (LV: a; b1; x2)
Foxg1-GOF (LV: a; b2; x1)
Foxg1-GOF / R (LV: a; b2; x2)
a LTR pPgk1 rtTA-M2 LTR
b1 LTR TREt PLAP LTR
b2 LTR TREt Foxg1 LTR
x1 LTR TREt PLAP LTR
x2 LTR pPgk1 JAK2V617F-V5 LTR
E
R=JAK2V617F-V5
Gfap+ cell frequency
ctr
R
Foxg1-GOF
Foxg1-GOF/R
n=4,4,4,4
F
E12.5 wt ncx precursors
dissociation
LV transduction*
2μg/ml doxy
DMEM/F12-GFs
analysis
0
10
days in vitro (DIV)
* ctr (LV:a;b1;c1;c1;d)
Foxg1-GOF (LV:a;b2;c1;c2;d)
a LTR pPgk1 rtTA-M2 LTR
b1 LTR TREt Foxg1 LTR
b2 LTR TREt PLAP LTR
c1 LTR pEF1α caStat3 LTR
c2 LTR TREt caSmad1 LTR
d LTR BMP-RE minCMV ZsGreen LTR
G
ctr
Foxg1-GOF
ZsGreen+ cell frequency
n=4,4
ZsGreen+ cell median fluorescence intensity
n=4,4

Fig. 5

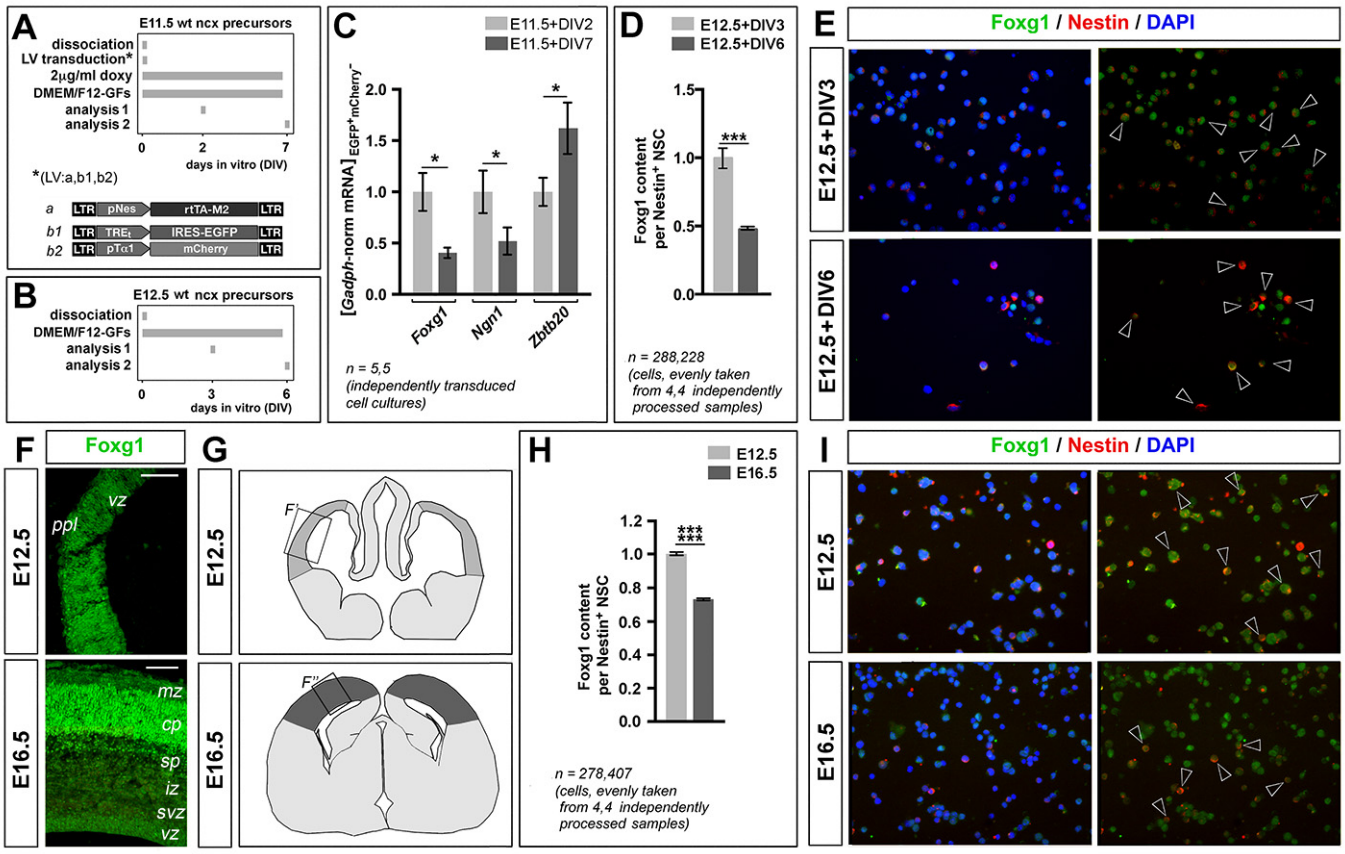
A
E11.5 wt ncx precursors
dissociation
LV transduction*
2µg/ml doxy
DMEM/F12-GFs
analysis 1
analysis 2
0
2
7
days in vitro (DIV)
*(LV:a,b1,b2)
a
LTR pNes rtTA-M2 LTR
b1
LTR TRE$_L$ IRES-EGFP LTR
b2
LTR pTα1 mCherry LTR
B
E12.5 wt ncx precursors
dissociation
DMEM/F12-GFs
analysis 1
analysis 2
0
3
6
days in vitro (DIV)
C
E11.5+DIV2
E11.5+DIV7
[Gadph-norm mRNA]EGFP+mCherry-
2.0
1.5
1.0
0.5
0.0
*
*
*
Foxg1
Ngn1
Zbtb20
n = 5,5
(independently transduced cell cultures)
D
E12.5+DIV3
E12.5+DIV6
Foxg1 content per Nestin+ NSC
1.5
1.0
0.5
0.0
***
n = 288,228
(cells, evenly taken from 4,4 independently processed samples)
E
Foxg1 / Nestin / DAPI
E12.5+DIV3
E12.5+DIV6
F
Foxg1
E12.5
E16.5
vz
ppl
mz
cp
sp
iz
svz
vz
G
E12.5
E16.5
F'
F''
H
E12.5
E16.5
Foxg1 content per Nestin+ NSC
1.2
1.0
0.8
0.6
0.4
0.2
0.0
***
***
n = 278,407
(cells, evenly taken from 4,4 independently processed samples)
I
Foxg1 / Nestin / DAPI
E12.5
E16.5

Fig. 6

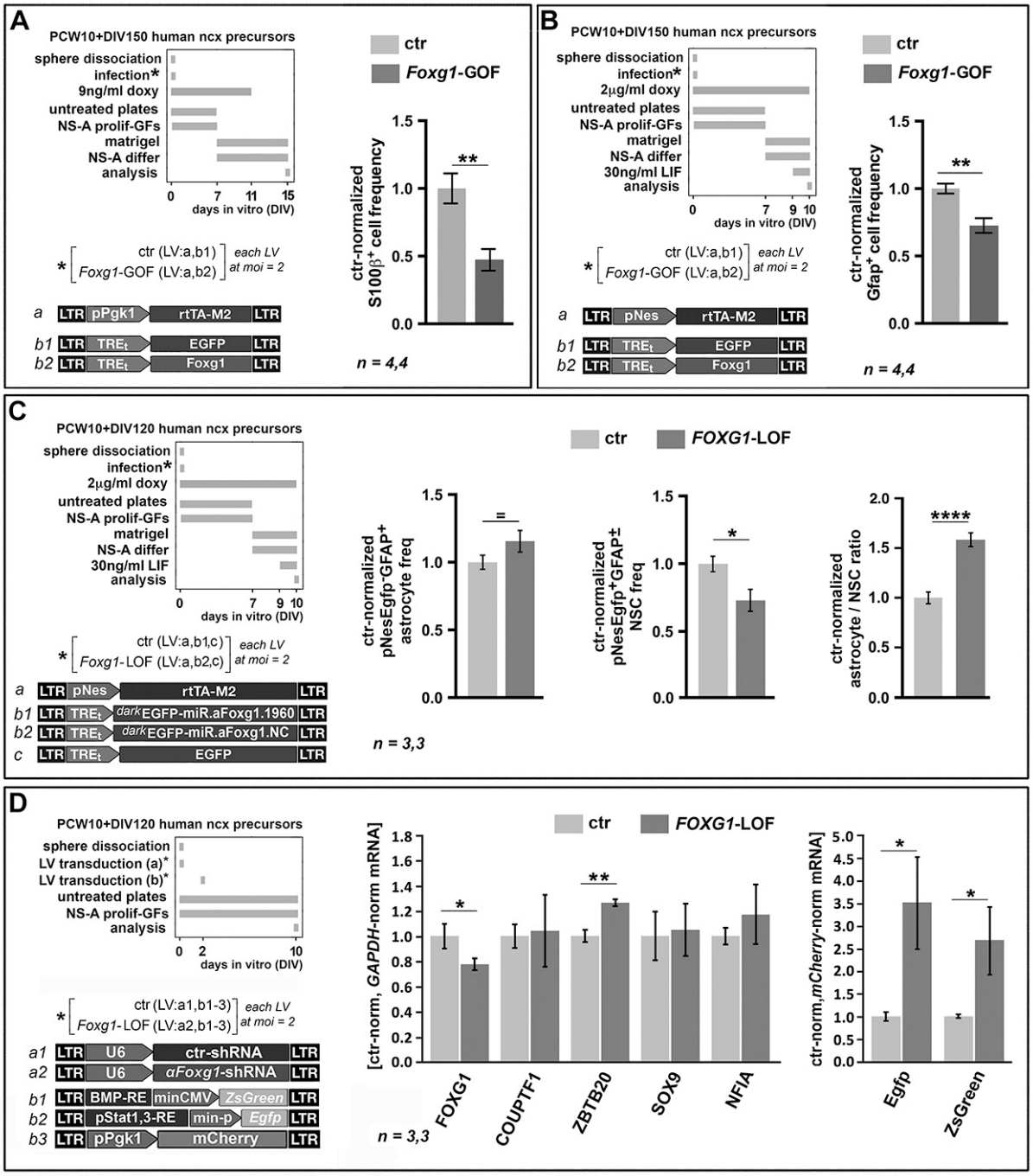
A
PCW10+DIV150 human ncx precursors
sphere dissociation
infection*
9ng/ml doxy
untreated plates
NS-A prolif-GFs
matrigel
NS-A differ
analysis
0 7 11 15
days in vitro (DIV)
* ctr (LV:a,b1) / Foxg1-GOF (LV:a,b2) each LV at moi = 2
a LTR pPgk1 rtTA-M2 LTR
b1 LTR TRE$_t$ EGFP LTR
b2 LTR TRE$_t$ Foxg1 LTR
ctr
Foxg1-GOF
ctr-normalized S100β$^+$ cell frequency
1.5
1.0
0.5
0.0
**
n = 4,4
B
PCW10+DIV150 human ncx precursors
sphere dissociation
infection*
2μg/ml doxy
untreated plates
NS-A prolif-GFs
matrigel
NS-A differ
30ng/ml LIF
analysis
0 7 9 10
days in vitro (DIV)
* ctr (LV:a,b1) / Foxg1-GOF (LV:a,b2) each LV at moi = 2
a LTR pNes rtTA-M2 LTR
b1 LTR TRE$_t$ EGFP LTR
b2 LTR TRE$_t$ Foxg1 LTR
ctr
Foxg1-GOF
ctr-normalized Gfap$^+$ cell frequency
1.5
1.0
0.5
0.0
**
n = 4,4
C
PCW10+DIV120 human ncx precursors
sphere dissociation
infection*
2μg/ml doxy
untreated plates
NS-A prolif-GFs
matrigel
NS-A differ
30ng/ml LIF
analysis
0 7 9 10
days in vitro (DIV)
* ctr (LV:a,b1,c) / Foxg1-LOF (LV:a,b2,c) each LV at moi = 2
a LTR pNes rtTA-M2 LTR
b1 LTR TRE$_t$ darkEGFP-miR.aFoxg1.1960 LTR
b2 LTR TRE$_t$ darkEGFP-miR.aFoxg1.NC LTR
c LTR TRE$_t$ EGFP LTR
ctr
FOXG1-LOF
ctr-normalized pNesEgfp$^-$GFAP$^+$ astrocyte freq
1.5
1.0
0.5
0.0
=
ctr-normalized pNesEgfp$^+$GFAP$^\pm$ NSC freq
1.5
1.0
0.5
0.0
*
ctr-normalized astrocyte / NSC ratio
2.0
1.5
1.0
0.5
0.0
****
n = 3,3
D
PCW10+DIV120 human ncx precursors
sphere dissociation
LV transduction (a)*
LV transduction (b)*
untreated plates
NS-A prolif-GFs
analysis
0 2 10
days in vitro (DIV)
* ctr (LV:a1,b1-3) / Foxg1-LOF (LV:a2,b1-3) each LV at moi = 2
a1 LTR U6 ctr-shRNA LTR
a2 LTR U6 αFoxg1-shRNA LTR
b1 LTR BMP-RE minCMV ZsGreen LTR
b2 LTR pStat1,3-RE min-p Egfp LTR
b3 LTR pPgk1 mCherry LTR
ctr
FOXG1-LOF
[ctr-norm, GAPDH-norm mRNA]
1.8
1.6
1.4
1.2
1.0
0.8
0.6
0.4
0.2
0.0
*
**
FOXG1
COUPTF1
ZBTB20
SOX9
NFIA
n = 3,3
ctr-norm,mCherry-norm mRNA]
5.0
4.5
4.0
3.5
3.0
2.5
2.0
1.5
1.0
0.5
0.0
*
*
Egfp
ZsGreen

Fig. 7

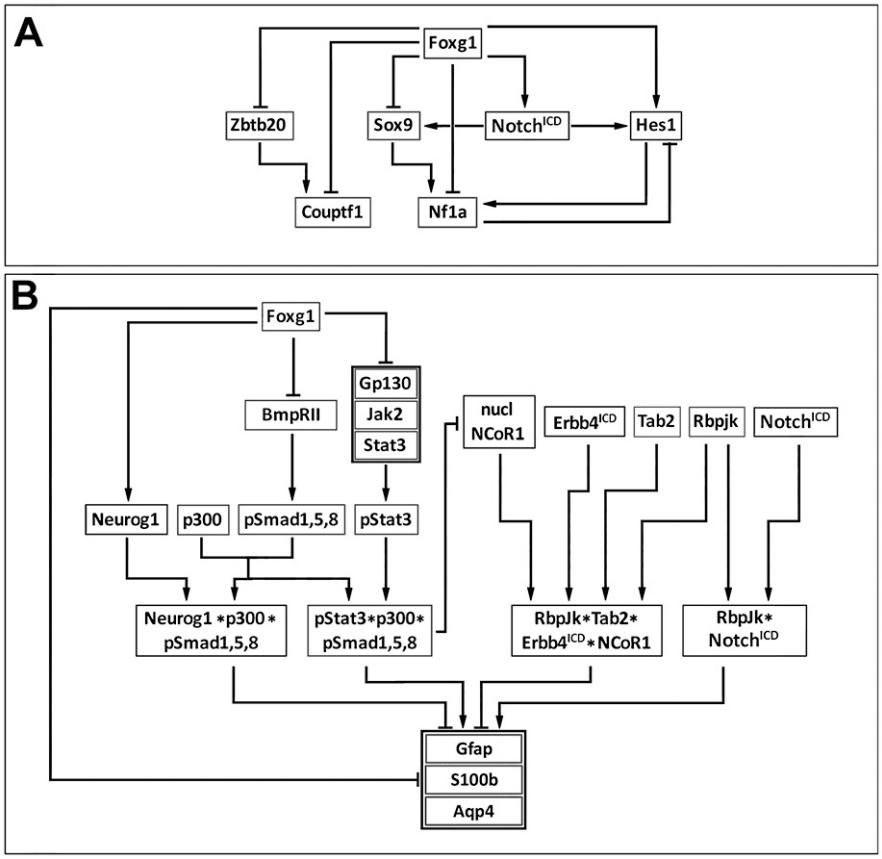
A
Foxg1
Zbtb20
Sox9
Notch^ICD
Hes1
Couptf1
Nf1a
B
Foxg1
Gp130
Jak2
Stat3
BmpRII
nucl
NCoR1
Erbb4^ICD
Tab2
Rbpjk
Notch^ICD
Neurog1
p300
pSmad1,5,8
pStat3
Neurog1 *p300* pSmad1,5,8
pStat3*p300* pSmad1,5,8
RbpJk*Tab2* Erbb4^ICD*NCoR1
RbpJk* Notch^ICD
Gfap
S100b
Aqp4